ARTICLES
https://doi.org/10.1038/s41590-018-0251-7
nature immunology

# Metabolic reprogramming of natural killer cells in obesity limits antitumor responses

Xavier Michelet[1,2,8], Lydia Dyck[3,8], Andrew Hogan[4], Roisin M. Loftus[3], Danielle Duquette[1], Kevin Wei[1], Semir Beyaz[2], Ali Tavakkoli[1], Cathriona Foley[3], Raymond Donnelly[3], Cliona O'Farrelly[3], Mathilde Raverdeau[3], Ashley Vernon[1], William Pettee[1], Donal O'Shea[4,5], Barbara S. Nikolajczyk[6], Kingston H. G. Mills[3], Michael B. Brenner[1,2], David Finlay[3,7] and Lydia Lynch[1,2,3,8]*

**Up to 49% of certain types of cancer are attributed to obesity, and potential mechanisms include overproduction of hormones, adipokines, and insulin. Cytotoxic immune cells, including natural killer (NK) cells and CD8$^+$ T cells, are important in tumor surveillance, but little is known about the impact of obesity on immunosurveillance. Here, we show that obesity induces robust peroxisome proliferator-activated receptor (PPAR)-driven lipid accumulation in NK cells, causing complete 'paralysis' of their cellular metabolism and trafficking. Fatty acid administration, and PPARα and PPARδ (PPARα/δ) agonists, mimicked obesity and inhibited mechanistic target of rapamycin (mTOR)-mediated glycolysis. This prevented trafficking of the cytotoxic machinery to the NK cell–tumor synapse. Inhibiting PPARα/δ or blocking the transport of lipids into mitochondria reversed NK cell metabolic paralysis and restored cytotoxicity. In vivo, NK cells had blunted antitumor responses and failed to reduce tumor growth in obesity. Our results demonstrate that the lipotoxic obese environment impairs immunosurveillance and suggest that metabolic reprogramming of NK cells may improve cancer outcomes in obesity.**

More than 1.9 billion adults are overweight or obese, representing over one third of the world-wide adult population[1]. The biggest health and economic burden of obesity is the large number of obesity-related co-morbidities. In addition to type 2 diabetes and cardiovascular disease, obesity is associated with an increased risk of cancer and infections[2–4]. Indeed, up to 49% of certain types of cancer are now attributed to obesity[3], and weight loss through bariatric surgery can reverse cancer risk[5]. Potential mechanisms for the increased risk of cancer associated with obesity include overproduction of hormones (for example, oestrogens), adipokines (for example, leptin), and insulin, which favor cell proliferation and tumor growth[6,7]. Peroxisome proliferator-activated receptors (PPARs) are transcriptional regulators of cellular metabolism. It has recently been shown that obesity induces a PPAR-driven lipid metabolism program in metastatic tumor cells, which enhances metastasis and tumor cell survival[8]. In intestinal stem cells, obesity-driven PPAR signaling enhances stemness and tumor progression[9]. However, despite the increasing attention to the role of the immune system and inflammation in obesity-driven insulin resistance, the impact of obesity-induced dysfunction on immunosurveillance and cancer risk is not well understood.

Natural killer (NK) cells have crucial roles in protective immunity against tumors and viral infections[10]. NK cells kill their targets through the directed secretion of lytic granules, which contain pore-forming perforin and apoptosis-inducing granzymes[11–13]. Cellular metabolism has a critical role in the function of immune cells. NK cells switch the balance of the core metabolic program from oxidative phosphorylation (OXPHOS) to glycolysis to meet the increased energy required to kill tumor cells[14,15], although the steps in the killing process that require this metabolic activation are unknown.

Humans and mice with obesity display numerical and functional defects in NK cells and have an increased risk of cancer and infections. As obesity is a state of altered metabolism, we investigated the effect of obesity on the cellular metabolism, gene expression, and function of NK cells, and its contribution to cancer development. Our data show that NK cell uptake of lipids from the environment in human obesity interfered with their cellular bioenergetics, inducing 'metabolic paralysis'. Lipid-induced metabolic defects caused NK cell incompetence by inhibiting trafficking of the cytotoxic machinery, leading to loss of antitumor functions in vitro and in vivo. Our data suggest that obesity targets immunometabolic pathways and that this may be partly responsible for the increased cancer and infection risks in obesity, and suggest that metabolic reprogramming may improve innate immunosurveillance in obesity.

## Results

**Obesity induces lipid metabolism in NK cells.** To better understand the effects of obesity on NK cells, we examined mouse models of diet-induced obesity. We performed transcriptional analysis of NK cells from mice fed a short-term (1 week) or long-term (8 weeks) high-fat diet (HFD), and compared this with transcriptional analysis of NK cells from mice fed a standard-fat diet (SFD). Gene expression analysis revealed that after just 1 week of HFD, NK cells upregulate 107 genes, the majority of which are related to lipid handling and metabolism (Fig. 1a). After 8 weeks of HFD, NK cell gene expression was changed substantially, with differential expression of 3,000 genes compared to SFD-fed mice (Fig. 1b).

[1]Brigham and Women's Hospital, Boston, MA, USA. [2]Harvard Medical School, Boston, MA, USA. [3]School of Biochemistry and Immunology & School of Medicine, Trinity College Dublin, Dublin, Ireland. [4]Human Health Institute Maynooth University, Kildare, Ireland. [5]Education Research Centre, St. Vincent's University Hospital, Dublin, Ireland. [6]Barnstable Brown Diabetes Center, University of Kentucky, Lexington, KY, USA. [7]School of Pharmacy and Pharmaceutical Sciences, Trinity Biomedical Sciences Institute, Trinity College Dublin, Dublin, Ireland. [8]These authors contributed equally: Xavier Michelet, Lydia Dyck, Lydia Lynch. *e-mail: llynch@bwh.harvard.edu

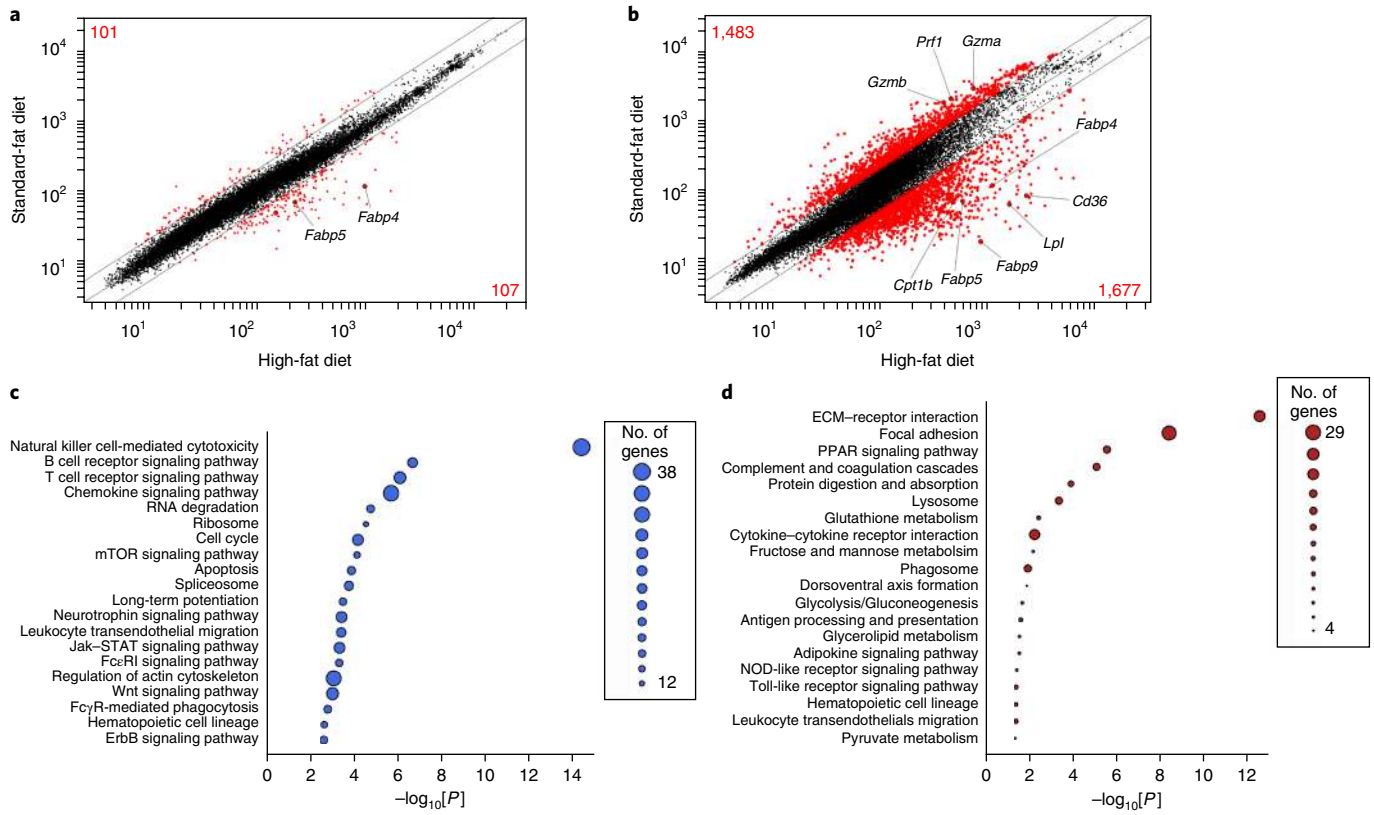


**Fig. 1 | NK cells from HFD mice show upregulation of lipid metabolism-related genes and downregulation of the killing machinery. a**,**b**, Microarray analysis of transcript expression in NK cells from male C57BL/6 mice after 1 week ($n$ = one sample, of three pooled mice) or 8 weeks ($n$ = two samples, three pooled mice per sample) on a HFD (**a**), compared to a SFD ($n$ = three samples, three pooled mice per sample) (**b**). Numbers indicate total genes overexpressed in HFD NK cells (bottom right) or under-represented (top left). **c**,**d**, Kegg pathway analysis of the downregulated (**c**) and upregulated (**d**) genes in HFD NK cells. The top 20 identified pathways are represented.

Many lipid handling and lipid metabolism genes were overexpressed in obesity, chief among them being *Ldlr*, *Cd36*, genes encoding fatty acid–binding proteins (FABPs), and *Cpt1b*. Genes highly downregulated included *Prf1* and genes encoding granzymes (Fig. 1b). Gene pathway analysis revealed that the most downregulated pathway was NK cell–mediated cytotoxicity. Genes involved in mechanistic target of rapamycin (mTOR) signaling were also downregulated (Fig. 1c). Highly upregulated pathways in NK cells in obesity included PPAR signaling and glycerolipid metabolism pathways (Fig. 1d). Indeed, the expression of genes involved in lipid-droplet formation and lipases (*Lipe* and *Plin2*), lipid and glycerol uptake (*Cd36*, *Lpl*, and *Lrp4*) and lipid metabolism (*Abca1*, *Scarb2*, and *Gyk*) was increased in NK cells from HFD mice. Interestingly, these were all PPARα/δ target genes (Fig. 1a,b). PPARα/δ are fatty acid–regulated transcription factors that control lipid metabolism and are turned on in the presence of free fatty acid (FFA) ligands. In obesity, there is a chronic elevation of FFA in the circulation[16,17]. These data suggest that obesity induces metabolic reprogramming in NK cells to lipid metabolism, which inhibits the expression of NK cell effector molecules.

**NK cells are dysfunctional in human obesity.** To investigate whether human obesity has the same effects as mouse obesity on NK cells, we studied NK cells from lean and obese age-matched individuals. Individuals with obesity were deficient in NK cell numbers and function. Consistent with previous studies[18–21], the frequency of circulating NK cells ($CD3^-CD56^+$) was significantly lower in obese individuals than in lean individuals (Fig. 2a). Moreover, we found that NK cells from obese individuals killed significantly fewer tumor cells (Fig. 2b) and produced significantly less interferon-γ (IFN-γ) compared with NK cells from lean individuals, as measured by flow cytometry (Fig. 2c) and by ELISA (Fig. 2d). Our studies with HFD in mice revealed a link between lipid metabolism and loss of cytotoxicity in NK cells. We next demonstrated that the same pathways were altered in NK cells in human obesity. Consistent with our findings in mice, we observed higher CD36 surface expression on NK cells from obese individuals than on those from lean individuals (Fig. 2e), suggestive of PPARα/δ pathway activation. Moreover, NK cells from obese individuals stained more strongly for lipids than those from lean donors (Fig. 2f). Microscopy revealed greater intracellular lipid droplet accumulation in NK cells from obese individuals than from lean individuals; NK cells from lean donors only stained for plasma membrane lipids (Fig. 2g). Thus, our results suggest that NK cells turn on PPARα lipid metabolism pathways in response to the lipid-rich environment in obesity. As in obese mice, NK cells from humans with obesity had lower expression of granzymes and perforin at the mRNA and protein level than lean individuals (Fig. 2h–j). Collectively, our data show that human obesity is associated with reduced NK cell cytotoxic effector functions.

**Lipid uptake inhibits human NK cell functions.** As NK cells from obese individuals displayed increased lipid accumulation, we investigated whether intracellular lipid accumulation is causally linked to the loss of function in human NK cells. There is a chronic elevation of FFA, particularly palmitate, in the circulation in obesity[16,17]. When human NK cells from lean controls were cultured with FFA (palmitate and/or oleate), they readily incorporated FFA from the media (Fig. 3a). Microscopy revealed that FFA-cultured NK cells had

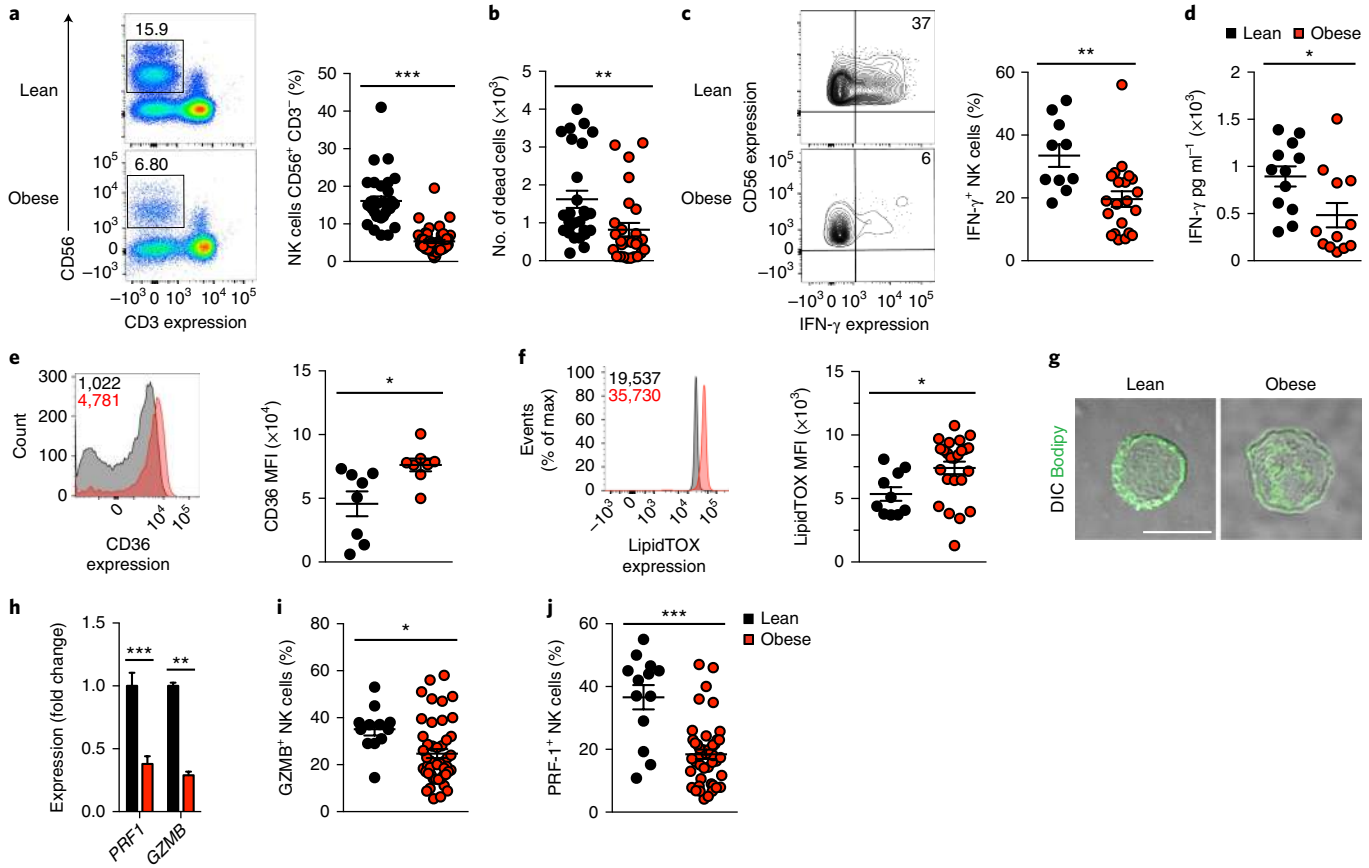


**Fig. 2 | Obesity leads to NK cell loss of function and lipid accumulation. a**, Dot plots and numbers of NK cells CD56$^+$ and CD3$^-$ from blood of lean ($n=32$) and obese ($n=50$) individuals. Numbers indicate the percentage of NK cells. Representative plots are shown. **b**, Cytotoxicity assay with NK cells from blood of lean ($n=27$) and obese ($n=27$) individuals co-incubated with target cells. **c**, Frequency of IFN-γ-positive NK cells stimulated with IL-2 and IL-12 (IL-2/IL-12) measured by flow cytometry ($n=10$ samples from lean individuals; $n=21$ samples from individuals with obesity). **d**, NK cells were stimulated with IL-2/IL-12 and supernatants were analyzed for IFN-γ by ELISA ($n=12$ samples from lean individuals, $n=12$ samples from individuals with obesity). **e**, CD36 expression in NK cells from blood of lean ($n=8$) and obese ($n=8$) individuals determined by flow cytometry. Numbers indicate mean fluorescence intensity (MFI). **f**, Lipids level of NK cells from lean ($n=9$) and obese ($n=24$) individuals measured by lipidTOX staining by flow cytometry. Numbers indicate MFI. **g**, Confocal images of NK cells isolated from the blood of lean and obese donors and stained with Bodipy 495/515. Representative of two independent experiments. **h**, *GZMB* and *PRF1* mRNA levels in NK cells isolated from blood of lean and obese individuals ($n=6$ per group). **i**,**j**, Frequency of PRF-1-positive (**i**) and GZMB-positive (**j**) NK cells from blood of lean ($n=13$) and obese ($n=45$) individuals. Scale bar represents 10 μm. Each symbol represents one individual. Short horizontal bars indicate the mean ± s.e.m. Statistics were calculated using a Student's unpaired *t*-test. $^*P<0.05$, $^{**}P<0.01$, $^{***}P<0.001$.

accumulated intracellular lipid droplets (Fig. 3b). Notably, NK cells that accumulated lipid droplets displayed a loss of perforin granules (Fig. 3b). The NK cells that accumulated the most lipids had little or no detectable perforin, whereas cells that took up fewer lipids had higher levels of perforin granules (Fig. 3b). Loss of perforin and granzyme B after FFA culture was detected by flow cytometry (Fig. 3c). Lipid accumulation in NK cells also led to loss of cytotoxicity against tumor cells (Fig. 3d and Supplementary Fig. 1a). FFA can be cytotoxic in certain cells, but at this concentration, lipid treatment did not affect the viability of NK cells (Supplementary Fig. 1b). NK cells pre-cultured with FFA also produced significantly less IFN-γ, in a dose-dependent manner (Fig. 3e and Supplementary Fig. 1c). We also tested whether other features of obesity could induce the loss of NK cell effector functions, including high glucose or high insulin concentrations, but unlike FFA culture, these conditions did not affect the ability of NK cells to kill target cells. Together, these results indicate that the lipid uptake and accumulation seen in NK cells from individuals with obesity blunts NK cell function.

**The mTORC1 pathway is impaired in obesity.** The protein kinase mechanistic target of rapamycin complex 1 (mTORC1) coordinates the metabolic activities of the cell in response to nutrients and growth factors[22]. Downstream targets and pathways of mTORC1 include granzyme expression[23] and glycolysis in T cells. The mTORC1 pathway is also crucial for NK cell function, particularly IFN-γ production[14,15], whereas less is known about mTORC1 and cytotoxic activity in NK cells. As mTORC1 activation is required for NK cell function, we reasoned that mTORC1 is inhibited in obesity or by lipid uptake. Primary human NK cells treated with the mTORC1 inhibitor rapamycin produced less IFN-γ (Supplementary Fig. 2a), confirming previous reports[14]. In addition, tumor killing by NK cells was significantly reduced in rapamycin-treated cells, and after treatment with SL0101-1, which inhibits the downstream target of mTORC1, the ribosomal S6 kinase (S6K) (Fig. 4a). These data confirm the requirement of mTORC1 for NK cell cytotoxic effector function.

Activation of mTORC1 is associated with its own phosphorylation and its localization at the lysosomal membrane. Confocal analysis revealed that mTOR localized with perforin and CD107a, illustrating that mTOR localizes with lytic granules (Supplementary Fig. 2b). NK cell activation with interleukin 2 (IL-2) and IL-12 resulted in increased phosphorylated mTOR (p-mTOR) expression,

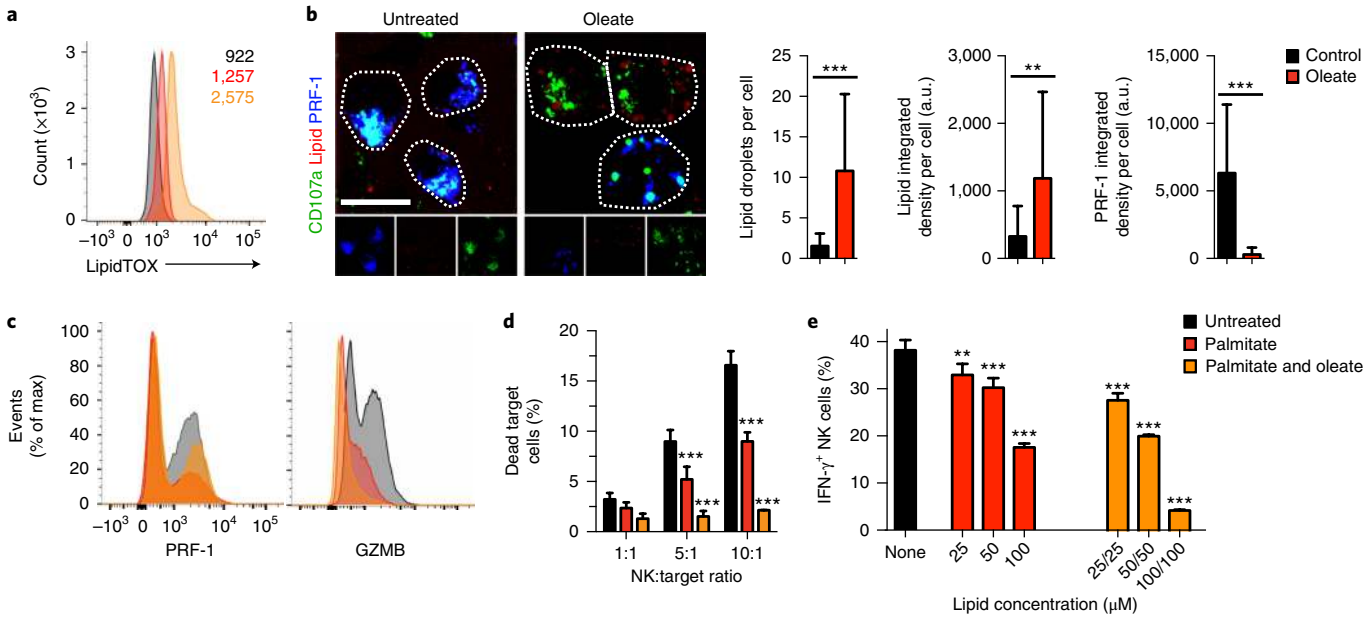


**Fig. 3 | Lipid uptake and accumulation leads to NK cell loss of function.** NK cells isolated from blood or YT-Indy cells were cultured with either palmitate (200 μM) or oleate (100 μM), or a mixture of palmitate (100 μM) and oleate (100 μM) for 36–48 h. **a**, Lipid levels of NK cells cultured with lipids. Numbers indicate MFI. **b**, YT-Indy cells cultured with lipids or not and stained for lipids, PRF-1 and CD107a. Dotted lines indicate cell boundaries. Image representative of 50 cells. Graphs show lipid droplet number and size, and perforin levels per cell. **c**, PRF-1 and GZMB expression by flow cytometry in NK cells cultured with and without lipids. **d**, NK cells cultured with lipids were co-incubated with K562 target cells for 1–2 h at various NK cell:target ratios. The percentage of dead target cells stained with propidium iodide (Pi) was then analyzed by flow cytometry ($n$ = six independent experiments). **e**, Numbers of IFN-γ$^+$ NK cells untreated or cultured with lipids at indicated concentrations and stimulated with IL-2/IL-12 ($n$ = six independent experiments). Statistics analyses were performed using a Student's unpaired $t$-test (**e**) and a two-way ANOVA followed by a Bonferroni test (**d**,**e**) to analyze each replicate. $^*P < 0.05$, $^{**}P < 0.01$, $^{***}P < 0.001$. In **a** and **c**, histograms of at least two independent experiments are shown.

which colocalized with lytic granules (lysosome-related organelles). As a control, mTOR was not phosphorylated in starvation media or in the presence of mTOR inhibitor Torin 1 (Fig. 4b). We next analyzed p-mTOR expression in lipid-treated NK cells by confocal microscopy. Compared with untreated NK cells, FFA-treated NK cells displayed a marked reduction in p-mTOR at lytic granules (Fig. 4c). We also measured mTORC1 activation via the downstream phosphorylation of S6 (p-S6) by S6K, by flow cytometry. Primary human NK cells from lean controls pre-treated with lipids displayed significantly less p-S6 after cytokine stimulation (Fig. 4d and Supplementary Fig. 2c) and after encountering tumor cells (Fig. 4e). We analyzed the level of mTORC1 activation in NK cells freshly isolated from obese and lean individuals. There was significantly less p-S6 in NK cells from obese compared to lean individuals after cytokine stimulation (Fig. 4f). Together, our findings show that a lipid-rich environment, such as in obesity, inhibits mTORC1 activation in human NK cells, which inhibits their effector function.

**NK cell metabolism is impacted negatively during obesity.** Cellular metabolism has a critical role in the effector function of immune cells, including NK cells. mTORC1 activation leads to an increase in aerobic glycolysis in NK cells, a requirement for full effector function[14,15]. As obesity is a state of altered metabolism, and mTORC1 activation is impaired in obesity, we investigated the effect of obesity on the cellular metabolism of human NK cells. We first measured the uptake of fluorescent glucose analog 2-NDBG in NK cells. NK cells pre-treated with lipids had significantly less 2-NBDG uptake when stimulated with cytokines (Fig. 5a) or with tumors than untreated NK cells (Supplementary Fig. 3a). Moreover, NK cells isolated ex vivo from individuals with obesity had significantly less 2-NDBG uptake when stimulated with cytokines than NK cells from lean individuals (Fig. 5b). In support of these findings, transcriptional data from NK cells of obese mice showed downregulation of many glycolytic genes compared with NK cells of lean mice (Supplementary Fig. 3b). To determine the effects of lipid uptake on bioenergetics in NK cells, we measured the oxygen consumption rate (OCR) and extracellular acidification rate (ECAR), which correspond to OXPHOS and aerobic glycolysis, respectively. We found that lipid pre-treatment significantly impaired the ability of NK cells to induce both glycolysis and OXPHOS after stimulation, and reduced their glycolytic capacity (Fig. 5c–e). Due to the inhibition of both glycolysis and OXPHOS, NK cells treated with lipids generated significantly less ATP (Fig. 5f). To confirm that these findings reflected the situation in human obesity, we measured bioenergetics of NK cells freshly isolated from obese and lean individuals. The basal metabolism of unstimulated NK cells is similarly low in both lean and obese individuals; however, cytokine stimulation of NK cells from lean individuals increased the rate of both glycolysis and OXPHOS to meet the increased metabolic demand, consistent with previous studies[14]. In contrast, stimulated NK cells from individuals with obesity had a substantially blunted metabolic response (Fig. 5g,h). Glycolysis and the glycolytic capacity were substantially lower in NK cells from individuals with obesity than lean individuals (Fig. 5g,i). Moreover, NK cells from obese individuals did not increase the rate of OXPHOS when stimulated, unlike NK cells from lean controls (Fig. 5h,i). We next asked whether similar metabolic defects were seen in NK cells in obese mice. Similar to humans, mice fed a HFD for 13 weeks had functionally defective NK cells that produced significantly less IFN-γ (Fig. 5j). NK cells isolated from obese mice displayed significant metabolic defects, including significantly lower p-S6 expression after activation (Fig. 5k), and significantly reduced glycolytic capacity, OXPHOS, and maximum respiration rate (Fig. 5l–q). Together, these results highlight that human and murine obesity are associated with severe

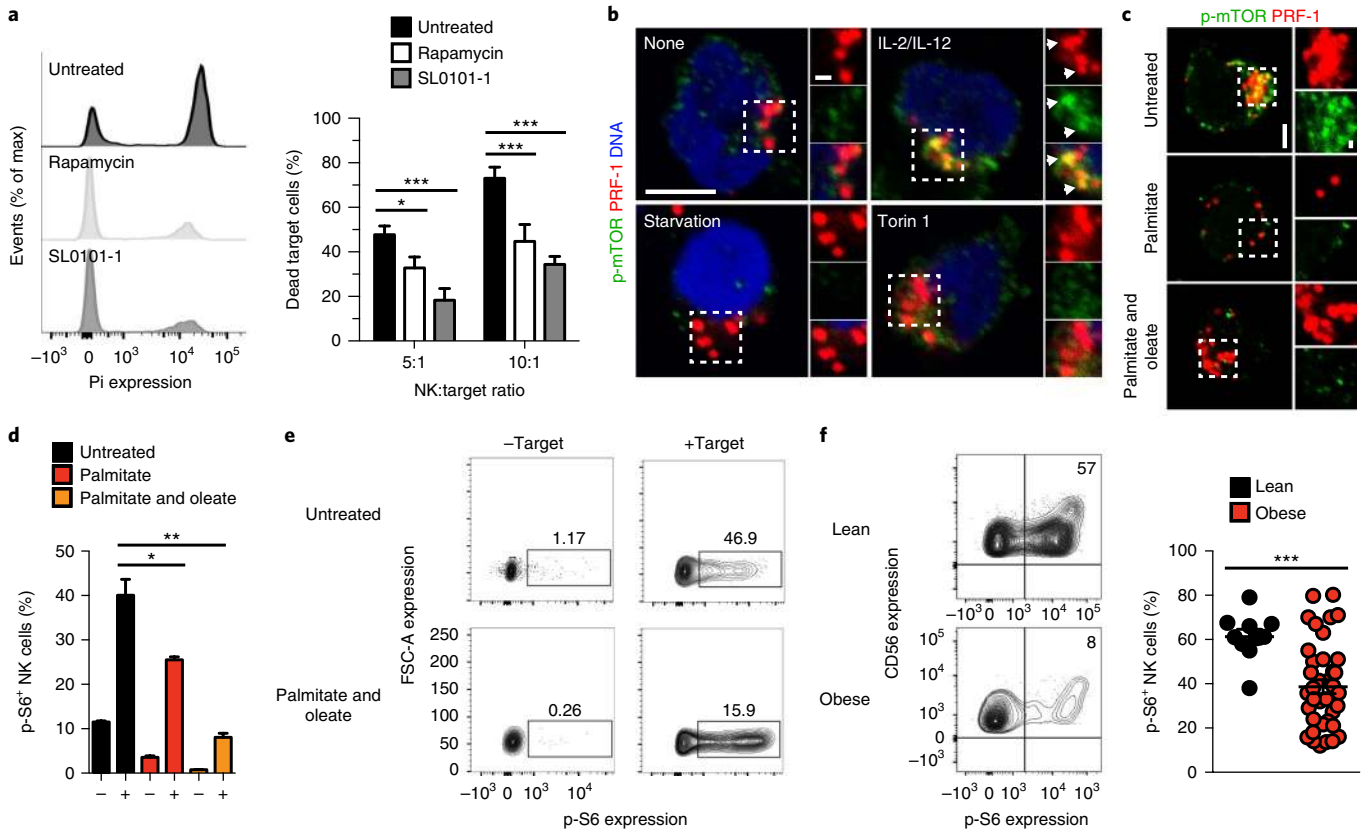


**Fig. 4 | Lipid accumulation during obesity impairs mTOR pathway. a**, Histograms and numbers of Pi$^+$ dead target cells of a cytotoxicity assay with NK cells pre-treated with rapamycin (20 nM) or SL0101-01 (10 nM) ($n$ = two independent experiments). **b**, Images of NK cells isolated from blood and stimulated with IL-2/IL-12 in control medium, in starvation conditions or cultured with Torin 1 (100 nM). Cells were stained for p-mTOR and PRF-1. Image representative of one experiment, with 50 cells. **c**, Images of NK cells treated with palmitate (200 μM), or palmitate (100 μM) and oleate (100 μM), and stained for p-mTOR and PRF-1. **d**, Percentage of p-S6$^+$ NK cells treated with lipids after IL-2/IL-12 stimulation. In **b** and **c**, images are representative of five independent experiments. **e**, Representative flow plots and combined data in graph of p-S6$^+$ NK cells treated with lipids after co-incubation with K562 target cells ($n$ = 3). Numbers in flow plots indicate the percentage of p-S6$^+$ NK cells. **f**, Histograms and numbers of p-S6$^+$ NK cells from lean ($n$ = 10) and obese ($n$ = 39) individuals. Numbers indicate the percentage of p-S6$^+$ NK cells. In **b** and **c**, scale bars represent 10 μm. Statistics were calculated using a two-way ANOVA followed by a Bonferroni test to analyze each replicate (**a**,**d**) and Student's unpaired $t$-test (**f**). $^*P < 0.05$, $^{**}P < 0.01$, $^{***}P < 0.001$.

cellular metabolic defects in NK cells, including a failure to activate both glycolytic and oxidative metabolic pathways, representing a type of metabolic paralysis. These metabolic and functional defects can be mimicked by culturing NK cells with FFAs, which is likely to underlie NK cell dysfunction in obesity.

**The PPARα/δ pathway contributes to NK cell defects in obesity.** Our data from mice and humans show that obesity-induced expression of PPAR target genes that encode proteins involved in lipid metabolism, increase lipid uptake and inhibition of the mTOR pathway. It has been reported that activation of the mTOR pathway inhibits PPAR lipid pathway targets[24–26]. Conversely, we investigated whether activation of PPAR pathways in NK cells can inhibit mTOR, leading to obesity-induced defects in NK cells. Human NK cells expressed *PPARA* and *PPARD*, but not *PPARG* (Fig. 6a). Treatment of NK cells from lean controls with PPARα and PPARδ agonists induced lipid uptake from the media, and significantly reduced the expression of perforin (Fig. 6b). Furthermore, when NK cells were cultured with FFA, addition of PPARα/δ antagonists prevented lipid accumulation and the loss of perforin (Fig. 6c). Thus, PPAR α/δ agonists mimicked the effects of obesity on NK cell function. We next tested whether PPARα/δ agonists affected NK metabolism. Treatment of NK cells from lean individuals with PPARα/δ agonists significantly inhibited p-S6, similar to FFA treatment, and PPARα/δ antagonists reversed the effects of FFA treatment (Fig. 6d). Furthermore, NK cells isolated from lean individuals treated with PPARα/δ agonists displayed lower glycolysis and glycolytic capacity than untreated NK cells (Fig. 6e). We next verified whether murine NK cells were similarly affected by PPAR pathway induction. NK cells isolated from spleens of lean mice treated with PPARα/δ agonists produced significantly less IFN-γ (Fig. 6f) and tended to have lower granzyme B expression (Fig. 6g) than untreated controls. Lean NK cells treated with PPARα/δ agonists displayed significantly blunted glycolytic capacity (Fig. 6h,j–l), and surprisingly, a significantly impaired maximal respiration rate (Fig. 6i,m,n) than untreated NK cells. Downstream signaling, including that of c-Myc (which is critical for NK cell metabolism) and p-S6, was inhibited in activated NK cells after treatment with PPARα/δ agonists (Fig. 6o). Thus, the upregulation of PPAR pathways in NK cells in obesity inhibits mTOR signaling, activation-induced metabolic reprogramming, and effector molecule expression in human and mouse NK cells.

**Mechanism of NK cell cytotoxic dysfunction in obesity.** Obesity-induced metabolic paralysis in NK cells results in loss of cytotoxic activity, but it is unknown which step (or steps) in the cytotoxic pathway require metabolic activation or are affected by obesity. NK cell cytotoxicity occurs in a stepwise controlled manner[11,12],

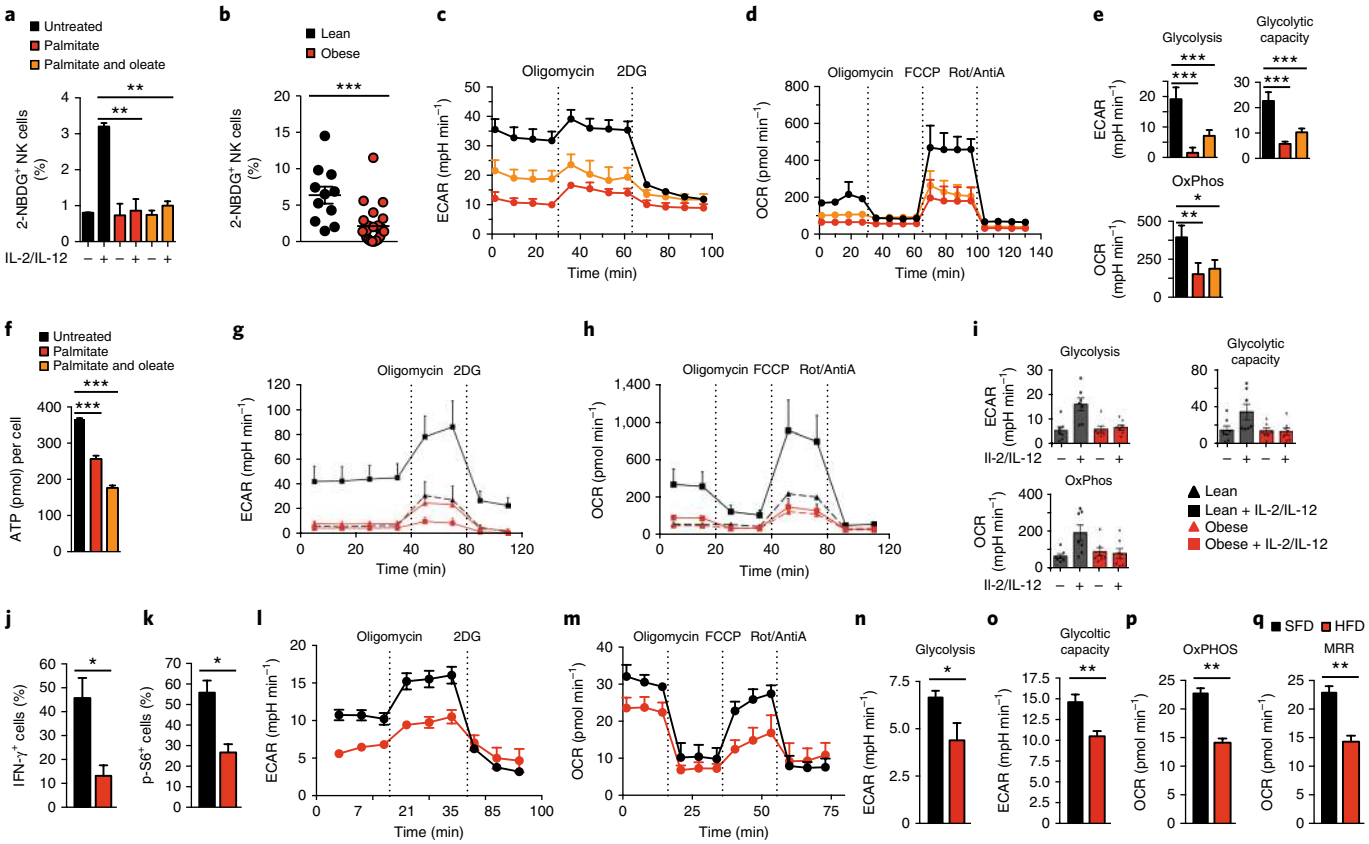


**Fig. 5 | Lipid accumulation during obesity negatively impacts NK cell metabolism. a**, Numbers of 2-NBDG$^+$ human NK cells treated with palmitate (200 μM), or palmitate (100 μM) and oleate (100 μM) after IL-2/IL-12 stimulation. **b**, Percentage of 2-NBDG$^+$ human NK cells following IL-2/IL-12 stimulation in lean ($n=11$) and obese ($n=25$) individuals. **c**–**e**, Real-time analysis of aerobic glycolysis (ECAR) (**c**) and OXPHOS (OCR) (**d**) in human NK cells cultured with palmitate (200 μM), or palmitate (100 μM) and oleate (100 μM). **e**, Analysis of ECAR and OCR in human NK cells cultured with lipids. **f**, ATP levels in human NK cells treated with lipids. **g**,**h**, Real-time analysis of ECAR (**g**) and OCR (**h**) in human NK cells isolated from blood of lean ($n=7$) and obese ($n=7$) individuals, unstimulated or stimulated with IL-2/IL-12. **i**, Analysis of ECAR and OCR in human NK cells stimulated with IL-2/IL-12. **j**–**q**, Mice were fed a HFD for 13 weeks. Mouse NK cells were isolated from blood of lean ($n=5$) and obese ($n=3$) mice, and stimulated with PMA, ionomycin and BFA for 4 h (**j**,**k**). IFN-γ production (**j**) and p-S6 levels (**k**) were measured by flow cytometry. NK cells were purified from the spleens of lean and obese mice before stimulation with IL-2/IL-12 for 20 h (**l**–**q**). Real-time analysis of ECAR (**l**) and OCR (**m**) in NK cells isolated from lean and obese mice ($n=$ four technical replicates, NK cells pooled from two mice per group, representative of two independent experiments). **n**–**q**, Analysis of glycolysis (**n**), glycolytic capacity (**o**), OXPHOS (**p**), and maximum respiratory rate (MRR) (**q**) in NK cells isolated directly from lean and obese mice and stimulated with IL-2/IL-12. Data are representative of at least two independent experiments. In **a** and **f**, error bars represent mean ± s.d. of three technical duplicates. In **l**–**q**, error bars represent mean ± s.e.m. of technical replicates ($n=$ three or four per experiment), results show data from two independent pooled experiments. In **c**–**e**, error bars represent mean ± s.d. of technical triplicates. In **b**, **g**, **h**, and **i**, error bars represent mean ± s.e.m. Statistics analyses were performed using a Student's unpaired *t*-test (**a**,**b**,**j**,**k**,**n**–**q**) and one-way ANOVA followed by a Bonferroni test (**e**,**f**,**i**) to analyze each replicate. $^*P<0.05$, $^{**}P<0.01$, $^{***}P<0.001$. Rot/AntiA, rotenone and antimycin A.

whereby NK cells form conjugates and a synapse with tumor cells, sending an activating signal to NK cells[27,28], inducing lytic granules to concentrate around the microtubule-organizing center (MTOC)[29,30]. Next, the lytic granules and MTOC are directed to the synapse, and their lytic content is released in a targeted manner into the synapse, which is essential for effective killing of tumor cells[31–33]. We investigated the stepwise process of cell killing in obesity to better understand the impact of altered metabolism, and hence obesity, on cytotoxicity.

First, we examined whether NK cells can recognize tumor cells in obesity, by measuring the presence of a synapse and the concentration of the adhesion protein CD2 at the synapse by confocal microscopy. Pre-treatment with lipids did not affect the ability of NK cells to form a conjugate and synapse with tumor targets (Fig. 7a), suggesting that NK cells do not require metabolic activation to recognize tumor cells or rearrange their actin filaments to form a synapse. We next measured polarization of the MTOC and found that lipid-treated NK cells were unable to polarize the MTOC towards the tumor cells, despite an intact synapse (Fig. 7a). The Golgi apparatus, which is associated with the MTOC[11,34], also did not polarize at the synapse (Fig. 7b). Similarly, NK cells from individuals with obesity formed a conjugate and synapse with tumor target cells but failed to polarize their MTOC and lytic granules to the synapse, whereas NK cells from lean controls were able to do so (Fig. 7c). Thus, obesity does not affect the ability of NK cells to recognize tumor cells or form an immune synapse but strongly impedes the ability of NK cells to direct lytic granules to the tumor cell and degranulate at the synapse, which is critical for efficient killing of tumor cells.

The inability of NK cells from obese individuals to mobilize their lytic machinery to the tumor, and their impaired mTORC1 activation, suggest that metabolic activation is required for this step. To test this, NK cells were treated with the mTOR inhibitors rapamycin or Torin 1 prior to incubation with tumors. Inhibition of mTOR did not affect the ability of NK cells to recognize or form conjugates with

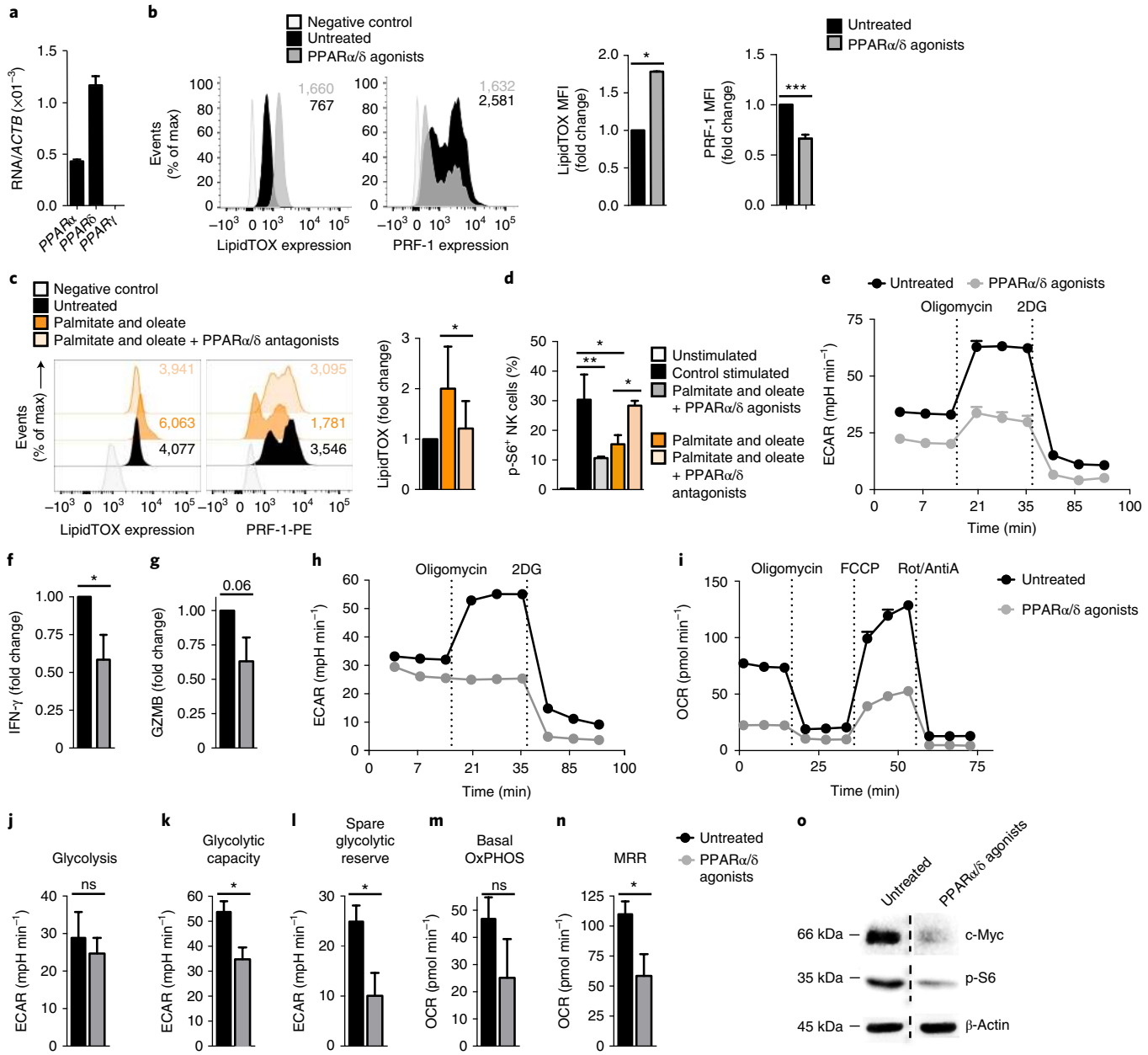


**Fig. 6 | Activation of the PPARα/δ pathway induces functional and metabolic defects in NK cells. a**, mRNA levels of *PPARA*, *PPARD*, and *PPARG* in human NK cells isolated from blood ($n=5$), relative to *ACTB* expression. **b**, Isolated human NK cells were cultured in the presence or absence of PPARα (10 μM) and PPARδ (10 μM) agonists for 5 days. Lipid levels and PRF-1 levels were analyzed by flow cytometry. Numbers indicate MFI ($n=6$). **c**,**d**, Lipid, PRF-1 and p-S6 levels of isolated human NK cells cultured with palmitate (100 μM) and oleate (100 μM), and PPARα (10 μM) and PPARδ (10 μM) antagonists ($n=6$). **e**, Real-time analysis of aerobic glycolysis (ECAR) in human NK cells cultured in the presence or absence of PPAR agonists (10 μM) for 5 days, before activation with the cytokines IL-2/IL-12 cytokines for 20 h ($n=$ four technical replicates, graph representative of four experiments). **f**–**n**, Mouse NK cells were expanded with low-dose IL-15 (10 ng ml$^{-1}$) in the presence or absence of PPARα (10 μM) and PPARδ (10 μM) agonists, before activation with the cytokines IL-2/IL-12 for 20 h. IFN-γ and granzyme B expression were measured by flow cytometry (**f**,**g**). Real-time analysis of aerobic glycolysis (ECAR) and OXPHOS (OCR) using the Seahorse metabolic flux analyzer (**h**–**n**). In **h**, $n=$ five technical replicates, graph representative of five experiments. In **i**–**n**, $n=$ five biological replicates. **o**, Immunoblot analysis measuring the expression of cMyc, p-S6 (S2335/236). β-actin was used as a loading control. Representative of four independent experiments. In all graphs, error bars represent mean ± s.e.m. Statistics were calculated using an unpaired Student's *t*-test (**b**,**f**,**g**,**j**–**n**) or a one-way ANOVA followed by a Bonferroni test (**c**,**d**) to analyze each replicate. $^*P<0.05$, $^{**}P<0.01$, $^{***}P<0.001$. ns, not significant.

tumor cells, but resulted in significantly fewer polarized NK cells (Fig. 7d and Supplementary Fig. 4). Blocking glycolysis in NK cells with the competitive glycolytic inhibitor 2-DG (2-deoxy-D-glucose) also inhibited NK cell polarization and tumor killing, despite normal tumor cell recognition and synapse formation (Fig. 7e). NK cell proliferation also requires MTOC polarization. We examined the effects of a lipid-rich environment in obesity and found that FFA treatment significantly impaired NK cell proliferation in mice and humans (Supplementary Fig. 5a,b). NK cells isolated from individuals with obesity did not expand in culture or when treated with PPAR agonists, unlike control NK cells (Supplementary Fig. 5c,d). Thus, lipid pathway induction and obesity impair the ability of NK

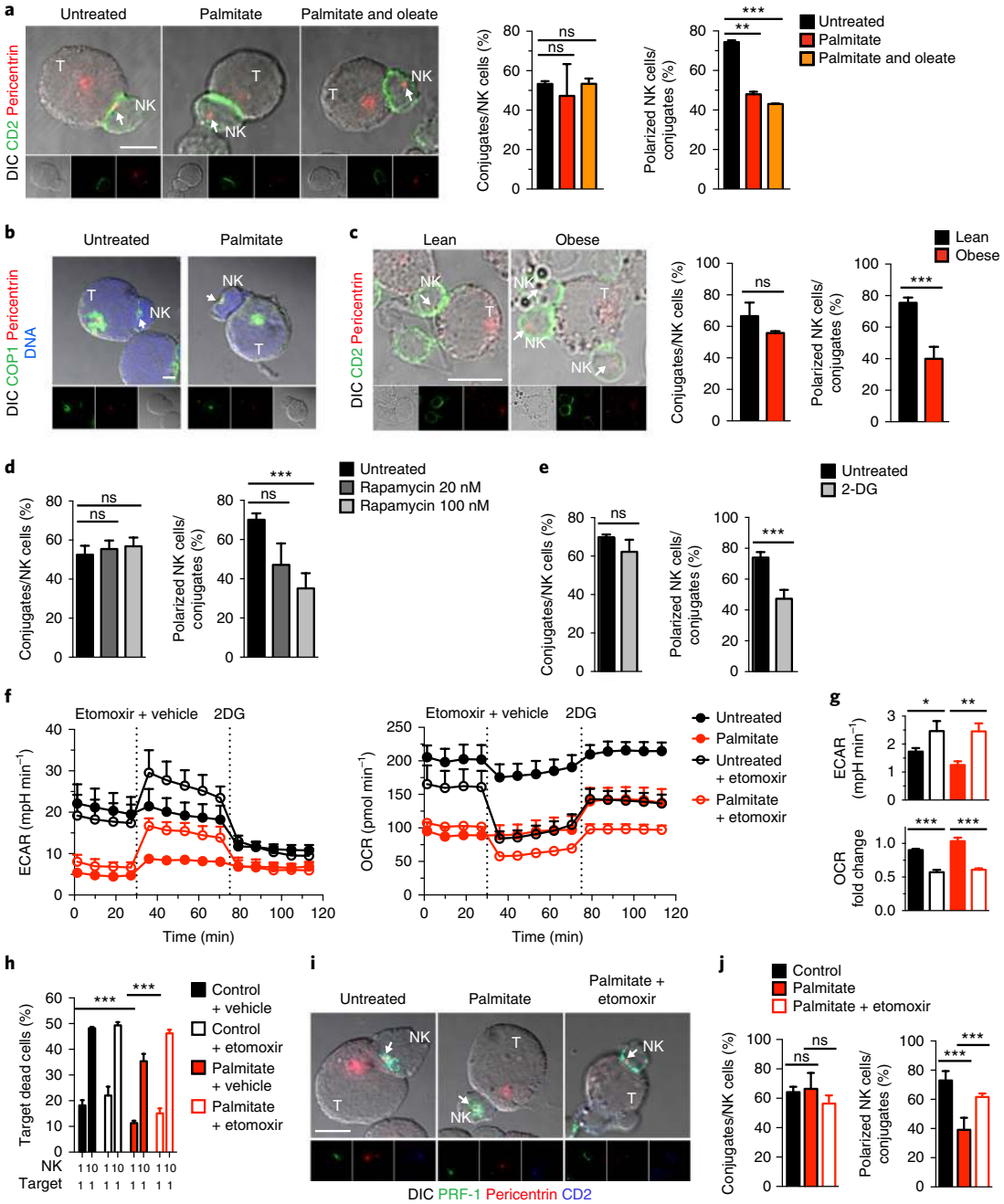


**Fig. 7 | The decreased ability of NK cells to kill tumor cells in obesity is related to a defect of lytic granule polarization and can be reversed with metabolic reprograming. a,b**, NK cells were co-incubated with target cells for 20 min, then conjugates of NK cells and target cells (NK:T) were fixed and stained for CD2 and pericentrin (**a**), or COP-1 and pericentrin (**b**). In **a** are shown images (left), frequency of NK:T conjugates (middle) and frequency of polarized NK cells of conjugated NK cells (right) pre-cultured with palmitate (200 μM), or palmitate (100 μM) and oleate (100 μM). In **b** are shown images of NK:T conjugates, cultured with or without palmitate (200 μM). Representative of three independent experiments. **c**, Images and frequency of NK:T conjugates and polarized NK cells from lean ($n=2$) and obese ($n=2$) individuals. **d**, Frequency of NK:T conjugates and polarized NK cells after rapamycin treatment (100 nM). **e**, Frequency of NK:T conjugates and polarized NK cells after 2DG (50 mM) treatment. **f**, Real-time analysis of aerobic glycolysis (ECAR) and OXPHOS (OCR) in NK cells cultured with palmitate (200 mM) followed by consecutive injections of (dotted vertical line), etomoxir (200 μM), or vehicle and 2-DG (30 mM). **g**, Rate of ECAR and OCR in NK cells cultured with palmitate (200 mM), and treated or not treated with etomoxir (200 μM). OCR rate is expressed as a fold change relative to the OCR measure before etomoxir or vehicle injection. **h**, Percentage of dead target cell after co-incubation with control or NK cells cultured with palmitate (200 mM) and pre-treated or not with etomoxir (200 μM) for 15 min. **i**, Images and number of NK:T conjugates with NK cells cultured with palmitate and pre-treated or not pre-treated with etomoxir. Conjugates were fixed and stained for PRF-1, pericentrin and CD2. In **a**, **b**, **c**, and **i**, white arrows denote the sub-localization of the MTOC. Scale bar represents 10 μm. Data are representative of two independent experiments. In **a**, mean ± s.d. of duplicates. Untreated, $n=118$ cells; palmitate, $n=178$ cells; palmitate and oleate, $n=135$ cells. In **d**, two independent experiments, mean ± s.d. of duplicates. Untreated, $n=115$ cells; rapamycin 20 mM, $n=116$ cells; rapamycin 100 mM, $n=114$ cells, In **e**, one experiment, mean ± s.d. of duplicates. Untreated, $n=133$ cells; 2-DG, $n=130$ cells. In **f**, **g**, and **h**, three independent experiments, mean ± s.d. of triplicates. In **i**, two independent experiments, mean ± s.d. of duplicates. In **c**, mean ± s.e.m. of cells from control ($n=2{,}143$ cells) and obese individuals ($n=2{,}213$ cells). Statistics were calculated using a Student's unpaired *t*-test (**g**,**h**) and chi-squared test (**a**,**c**,**d**,**e**,**j**). $^{*}P<0.05$, $^{**}P<0.01$, $^{***}P<0.001$. ns, not significant.

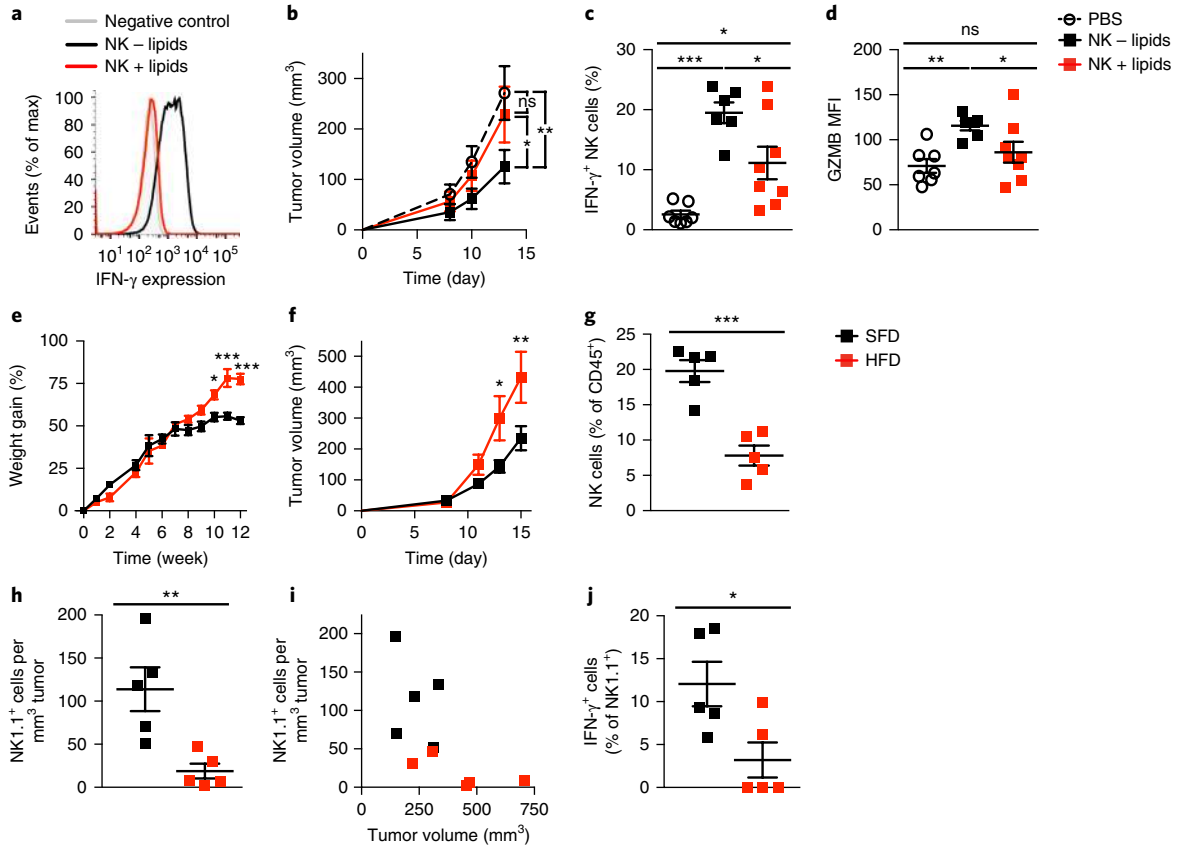


**Fig. 8 | Lipid uptake reduces NK cell antitumor activity in vivo. a**, Level of IFN-γ expression of splenic NK cells treated or not treated with lipids (palmitate and oleate) for 24 h prior to cytokine stimulation with IL-12, IL-15 and IL-18. Representative of three independent experiments. **b**–**d**, Mice bearing B16 tumors were injected with splenic cytokine-stimulated NK cells pre-treated or not pre-treated with lipids for 24 h. Tumor growth in mice is shown after NK cell transfer ($n = 15$ mice for each group, ± s.e.m, pooled results from two independent experiments) (**b**). IFN-γ expression (**c**) and GZMB expression (**d**) in NK cells from tumor-draining lymph nodes are shown (PBS = 7 mice, NK − lipids = 5 mice, NK + lipids = 8 mice). **e**–**j**, Mice were fed with a HFD (45% lard) for 12 weeks and at week 10, B16 tumor were injected s.c. into the flank ($n = 5$ mice per group). Data show weight gain (**e**) and tumor growth (**f**). On day 15 post tumor induction, tumors were isolated and the NK cell frequency (**g**), density (**h**,**i**) and IFN-γ production were analyzed by flow cytometry (**j**). In **c**, **d**, and **g**–**j**, each symbol represents one individual mouse. Small horizontal bars indicate the mean (±s.e.m). Statistics were calculated using a Student's unpaired *t*-test (**c**,**d**,**g**,**h**,**j**) or a two-way ANOVA followed by a Bonferroni test (**b**,**e**,**f**) to analyze each replicate. $^*P < 0.05$, $^{**}P < 0.01$, $^{***}P < 0.001$. ns, not significant.

cells to proliferate, which may partly explain the reduced NK cell numbers in obesity. Together, our results demonstrate that obesity-induced NK cell functional defects are due to induction of lipid pathways, impaired metabolism, and mTORC1 inhibition, which inhibit intracellular trafficking in NK cells.

**Reversal of metabolic defects restores NK cell cytotoxicity.** Our data suggest that reversing metabolic defects in NK cells in obesity might restore cytotoxicity. The fatty acid translocase gene *Cpt1*, which transports fatty acids to the mitochondria, was among the lipid-related genes upregulated in obesity (Supplementary Fig. 3b). Blocking fatty acid transport can induce a metabolic switch from OXPHOS to glycolysis. Although both glycolysis and OXPHOS were defective in obesity, previous studies have shown that glycolysis has an important role in NK effector functions. We therefore reasoned that blocking CPT1b may increase glycolysis, and thereby restore NK cell cytotoxicity. Bioenergetics of NK cells treated with lipids were measured in the presence of the CPT1b inhibitor etomoxir. Although the glycolytic rate was blunted after lipid treatment, the addition of etomoxir significantly increased the rate of glycolysis in NK cells (Fig. 7f,g). As a control, we measured the OCR after etomoxir treatment and demonstrated that this was reduced as expected due to blocking of CPT1b (Fig. 7f,g). Importantly, etomoxir restored NK cell cytotoxicity (Fig. 7h). If the defect in cytotoxicity was due to inability to activate glycolysis to polarize lytic granules upon tumor encounter, then restoring glycolysis should restore the ability to polarize the MTOC and lytic machinery to the synapse. Indeed, etomoxir treatment did not change the number of NK cell–tumor conjugates; however, it significantly increased the percentage of polarized NK cells with their MTOC and lytic granules at the immunological synapse and therefore increased tumor killing (Fig. 7i,j). Thus, metabolic defects associated with lipid uptake can be restored, and this meets the metabolic requirements for NK cells to assume their cytotoxic function.

**Lipid-treated NK cells fail to control tumor growth in vivo.** Lipid accumulation was seen in NK cells in vivo in both human and murine obesity, and lipid accumulation led to loss of cytotoxic function in vitro. We next determined the effect of obesity-induced defects on tumor growth in vivo. Lipid treatment of splenic NK cells completely inhibited their ability to produce IFN-γ when stimulated with IL-12, IL-15, and IL-18 (Fig. 8a). Next, we asked whether lipid uptake inhibited the ability of NK cells to efficiently kill tumor cells in vivo, using a B16F10 melanoma model. Lipid-treated or control NK cells were activated with IL-12, IL-15, and IL-18, and were injected peritumorally into B16 tumor–bearing mice on days 3, 7,

and 11 post tumor induction. Transfer of stimulated control NK cells significantly reduced the tumor burden, whereas stimulated lipid-treated NK cells had no impact on tumor burden; there was no difference in tumor growth in mice injected with lipid-treated NK cells or mice injected with PBS buffer (Fig. 8b). We next analyzed lymphocytes from draining lymph nodes 7 days after the final NK cell injection. NK cells that had been pre-treated with lipids showed lower IFN-γ production and granzyme B expression in vivo, compared to control NK cells (Fig. 8c,d). Thus, lipid accumulation in NK cells impairs NK cell effector functions in vivo, resulting in a failure to reduce tumor growth. To examine the effects of obesity on tumor growth in vivo, we fed wild-type mice a HFD for 12 weeks and injected B16 cells in week 10. As expected, weight gain was significantly greater in HFD-fed mice (Fig. 8e). Obese mice had more rapid and severe tumor development than lean mice (Fig. 8f). We next examined the tumor-infiltrating lymphocytes and found that NK cells were significantly reduced in tumors in obese mice, both in percentage and in density (Fig. 8g,h) Furthermore, the tumor size was inversely correlated with the number of tumor-infiltrating NK cells (Fig. 8i), confirming our observation that NK cells have a protective effect against tumor growth. In line with the data that obesity inhibits NK cell functions, we found that the NK cell compartment in the tumors of obese mice was functionally defective, producing significantly less IFN-γ than in the tumors of lean mice (Fig. 8j). Together, our data show that the metabolic and functional defects in NK cells induced by obesity impair effective antitumor responses in vivo, resulting in increased tumor growth in obesity.

## Discussion

It is now well accepted that obesity causes immune dysregulation, but most studies have so far focused on increased inflammation that interferes with insulin signaling and ultimately contributes to type 2 diabetes. Our findings show that in addition to increased inflammation, obesity also impairs antitumor activity by cytotoxic lymphocytes. Chronic elevation of circulating FFAs, including palmitate, is a hallmark of obesity and has been linked to the development of insulin resistance[17,35]. We show that in obesity NK cells also take up lipids from the environment, which interferes with their cellular bioenergetics, inducing metabolic paralysis. This occurs through interference with mTOR–PPAR pathways. When mTOR is active, PPARα/δ-mediated lipid pathways are inhibited, but in obesity, the PPARα/δ target genes are highly upregulated, potentially as a mechanism to deal with lipotoxic environments. However, upregulation of PPARα/δ inhibits mTOR-mediated glycolysis as well as downstream transcription of cytotoxic granules and IFN-γ production. We also show that the mTOR pathway and glycolysis are essential for the step in the NK cell cytotoxic process that requires polarization of the MTOC and lytic granules to the tumor synapse, enabling efficient tumor killing. Thus, we have identified a mechanism of NK cell dysfunction in murine and human obesity, whereby NK cells isolated directly ex vivo from individuals with obesity lack the metabolic requirements to kill tumor cells. Furthermore, in mouse models, lipid-induced metabolic dysfunction was sustained in vivo and resulted in increased tumor burden.

It was found recently that NK ILC1 cells are resident and abundant in adipose tissue and respond dynamically to changes in the diet and the ensuing weight loss or weight gain[36–39]. NK cells that infiltrate adipose tissue in obesity[36], together with adipose-resident NK cells, have an important role in regulating adipose macrophage populations through cytokine production[37,38] and direct cytotoxicity[36]. Some of these studies highlighted the dysregulation of NK cells in obesity, suggesting that they contribute to inflammation and insulin resistance. In addition, in obese adipose tissue, NK cell cytotoxic functions against 'stressed' macrophages were also impaired. These studies highlight the dysregulation in adipose NK cells induced by obesity, leading to an overall inflammatory environment. Thus, obesity causes a seemingly paradoxical state of chronic low-grade inflammation coupled with immunosuppression, similar to that reported for chronic inflammation and immunosuppression in other situations, including cancer[40], spinal cord injury[41] and sepsis[42]. Indeed, it has been found that sepsis-induced inflammation and immunosuppression are caused by metabolic paralysis characterized by loss of both glycolytic and oxidation metabolism[43], similar to our findings in human obesity.

The realization that metabolism controls cell function in health and disease has led to a resurgent interest in cellular metabolism, with the ultimate goal of targeting metabolism therapeutically. Our study highlights the interdependence of cellular and systemic metabolism in immune regulation. The metabolic state of the organism affects the immune system through altered fuel supplies and cellular metabolism used by immune cells. This in turn regulates immune cell function, which we now know can subsequently regulate whole-body metabolism, such that an immunometabolic loop exists between systemic and cellular metabolism in the organism. Our data raise the question of whether other scenarios of metabolic disorder may affect NK cells in a similar way. NK cells have a central role in antitumor immunity; however, a recent study of 18,000 tumor cases showed that resting or senescent NK cells in the tumor environment are associated with poor prognosis[44]. Our study provides insight into the metabolic requirements of NK cells to effectively kill tumor cells at the cellular level. In the tumor microenvironment where the tumor is consuming glucose and has high rates of glycolysis, tumor-infiltrating NK cells may be glucose deprived, leading to their inability to turn on mTORC1 and polarize lytic granules. Studies have suggested that treatment with rapamycin, which inhibits mTORC1 and glycolysis, may be a useful strategy to restrict tumor growth, as it would limit the increased Warburg glycolytic metabolism in tumor cells. However, our data suggest that rapamycin treatment, if untargeted, would also impair the ability of NK cells to kill tumor cells. Furthermore, our data show that obesity is analogous to rapamycin treatment in terms of NK cell functions. This is likely to impact the ability of the innate immune system to respond to foreign or damaged cells, and may partly explain the increased risk of infection and cancer in individuals with obesity[3,4].

Despite increased public awareness, the prevalence of obesity and related diseases continues to rise. Therefore, there is an urgent need to understand the pathways by which obesity leads to other diseases, and to develop new strategies to prevent their progression. Our results highlight immunometabolic pathways as a target to reverse immune defects in obesity and suggest that metabolic reprogramming of NK cells may improve their antitumor activity in human obesity.

## Online content

Any methods, additional references, Nature Research reporting summaries, source data, statements of data availability and associated accession codes are available at https://doi.org/10.1038/s41590-018-0251-7.

Received: 27 September 2017; Accepted: 2 October 2018;
Published online: 12 November 2018

## References

1. Global status report on noncommunicable diseases 2014 (WHO, 2004).
2. Calle, E. E. & Kaaks, R. Overweight, obesity and cancer: epidemiological evidence and proposed mechanisms. *Nat. Rev. Cancer* **4**, 579–591 (2004).
3. Renehan, A. G., Tyson, M., Egger, M., Heller, R. F. & Zwahlen, M. Body-mass index and incidence of cancer: a systematic review and meta-analysis of prospective observational studies. *Lancet* **371**, 569–578 (2008).
4. Falagas, M. E. & Kompoti, M. Obesity and infection. *Lancet. Infect. Dis.* **6**, 438–446 (2006).
5. Sjostrom, L. et al. Effects of bariatric surgery on cancer incidence in obese patients in Sweden (Swedish Obese Subjects Study): a prospective, controlled intervention trial. *Lancet Oncol.* **10**, 653–662 (2009).

6. Renehan, A. G., Zwahlen, M. & Egger, M. Adiposity and cancer risk: new mechanistic insights from epidemiology. *Nat. Rev. Cancer* **15**, 484–498 (2015).
7. Park, J., Morley, T. S., Kim, M., Clegg, D. J. & Scherer, P. E. Obesity and cancer mechanisms underlying tumour progression and recurrence. *Nat. Rev. Endocrinol.* **10**, 455–465 (2014).
8. Pascual, G. et al. Targeting metastasis-initiating cells through the fatty acid receptor CD36. *Nature* **541**, 41–45 (2017).
9. Beyaz, S. et al. High-fat diet enhances stemness and tumorigenicity of intestinal progenitors. *Nature* **531**, 53–58 (2016).
10. Vivier, E., Tomasello, E., Baratin, M., Walzer, T. & Ugolini, S. Functions of natural killer cells. *Nat. Immunol.* **9**, 503–510 (2008).
11. Mace, E. M. et al. Cell biological steps and checkpoints in accessing NK cell cytotoxicity. *Immunol. Cell Biol.* **92**, 245–255 (2014).
12. Orange, J. S. Formation and function of the lytic NK-cell immunological synapse. *Nat. Rev. Immunol.* **8**, 713–725 (2008).
13. Chowdhury, D. & Lieberman, J. Death by a thousand cuts: granzyme pathways of programmed cell death. *Annu. Rev. Immunol.* **26**, 389–420 (2008).
14. Donnelly, R. P. et al. mTORC1-dependent metabolic reprogramming is a prerequisite for NK cell effector function. *J. Immunol.* **193**, 4477–4484 (2014).
15. Marcais, A. et al. The metabolic checkpoint kinase mTOR is essential for IL-15 signaling during the development and activation of NK cells. *Nat. Immunol.* **15**, 749–757 (2014).
16. Bjorntorp, P., Bergman, H. & Varnauskas, E. Plasma free fatty acid turnover rate in obesity. *Acta Med. Scand.* **185**, 351–356 (1969).
17. Jensen, M. D., Haymond, M. W., Rizza, R. A., Cryer, P. E. & Miles, J. M. Influence of body fat distribution on free fatty acid metabolism in obesity. *J. Clin. Invest.* **83**, 1168–1173 (1989).
18. Lynch, L. A. et al. Are natural killer cells protecting the metabolically healthy obese patient? *Obesity (Silver Spring)* **17**, 601–605 (2009).
19. O'Shea, D., Cawood, T. J., O'Farrelly, C. & Lynch, L. Natural killer cells in obesity: impaired function and increased susceptibility to the effects of cigarette smoke. *PloS ONE* **5**, e8660 (2010).
20. Jahn, J. et al. Decreased NK cell functions in obesity can be reactivated by fat mass reduction. *Obesity (Silver Spring)* **23**, 2233–2241 (2015).
21. Perdu, S. et al. Maternal obesity drives functional alterations in uterine NK cells. *JCI Insight* **1**, e85560 (2016).
22. Laplante, M. & Sabatini, D. M. mTOR signaling in growth control and disease. *Cell* **149**, 274–293 (2012).
23. Finlay, D. K. et al. PDK1 regulation of mTOR and hypoxia-inducible factor 1 integrate metabolism and migration of $CD8^+$ T cells. *J. Exp. Med.* **209**, 2441–2453 (2012).
24. Wang, R. & Green, D. R. Metabolic checkpoints in activated T cells. *Nat. Immunol.* **13**, 907–915 (2012).
25. Sengupta, S., Peterson, T. R., Laplante, M., Oh, S. & Sabatini, D. M. mTORC1 controls fasting-induced ketogenesis and its modulation by ageing. *Nature* **468**, 1100–1104 (2010).
26. Lefebvre, P., Chinetti, G., Fruchart, J. C. & Staels, B. Sorting out the roles of PPAR alpha in energy metabolism and vascular homeostasis. *J. Clin. Invest.* **116**, 571–580 (2006).
27. Barber, D. F., Faure, M. & Long, E. O. LFA-1 contributes an early signal for NK cell cytotoxicity. *J. Immunol.* **173**, 3653–3659 (2004).
28. Mace, E. M., Monkley, S. J., Critchley, D. R. & Takei, F. A dual role for talin in NK cell cytotoxicity: activation of LFA-1-mediated cell adhesion and polarization of NK cells. *J. Immunol.* **182**, 948–956 (2009).
29. James, A. M. et al. Rapid activation receptor- or IL-2-induced lytic granule convergence in human natural killer cells requires Src, but not downstream signaling. *Blood* **121**, 2627–2637 (2013).
30. Mentlik, A. N., Sanborn, K. B., Holzbaur, E. L. & Orange, J. S. Rapid lytic granule convergence to the MTOC in natural killer cells is dependent on dynein but not cytolytic commitment. *Mol. Biol. Cell* **21**, 2241–2256 (2010).
31. Liu, D., Martina, J. A., Wu, X. S., Hammer, J. A. 3rd & Long, E. O. Two modes of lytic granule fusion during degranulation by natural killer cells. *Immunol. Cell Biol.* **89**, 728–738 (2011).
32. Menager, M. M. et al. Secretory cytotoxic granule maturation and exocytosis require the effector protein hMunc13-4. *Nat. Immunol.* **8**, 257–267 (2007).
33. Tuli, A. et al. Arf-like GTPase Arl8b regulates lytic granule polarization and natural killer cell-mediated cytotoxicity. *Mol. Biol. Cell* **24**, 3721–3735 (2013).
34. Kupfer, A., Dennert, G. & Singer, S. J. Polarization of the Golgi apparatus and the microtubule-organizing center within cloned natural killer cells bound to their targets. *Proc. Natl Acad. Sci. USA* **80**, 7224–7228 (1983).
35. Boden, G. & Shulman, G. I. Free fatty acids in obesity and type 2 diabetes: defining their role in the development of insulin resistance and beta-cell dysfunction. *Eur. J. Clin. Invest.* **32**, 14–23 (2002).
36. Boulenouar, S. et al. Adipose type one innate lymphoid cells regulate macrophage homeostasis through targeted cytotoxicity. *Immunity* **46**, 273–286 (2017).
37. Wensveen, F. M. et al. NK cells link obesity-induced adipose stress to inflammation and insulin resistance. *Nat. Immunol.* **16**, 376–385 (2015).
38. O'Sullivan, T. E. et al. Adipose-resident group 1 innate lymphoid cells promote obesity-associated insulin resistance. *Immunity* **45**, 428–441 (2016).
39. Lee, B. C. et al. Adipose natural killer cells regulate adipose tissue macrophages to promote insulin resistance in obesity. *Cell Metab.* **23**, 685–698 (2016).
40. Muller, A. J. et al. Chronic inflammation that facilitates tumor progression creates local immune suppression by inducing indoleamine 2,3 dioxygenase. *Proc. Natl Acad. Sci. USA* **105**, 17073–17078 (2008).
41. Allison, D. J. & Ditor, D. S. Immune dysfunction and chronic inflammation following spinal cord injury. *Spinal Cord* **53**, 14–18 (2015).
42. Gentile, L. F. et al. Persistent inflammation and immunosuppression: a common syndrome and new horizon for surgical intensive care. *J. Trauma Acute Care Surg.* **72**, 1491–1501 (2012).
43. Cheng, S. C. et al. Broad defects in the energy metabolism of leukocytes underlie immunoparalysis in sepsis. *Nat. Immunol.* **17**, 406–413 (2016).
44. Gentles, A. J. et al. The prognostic landscape of genes and infiltrating immune cells across human cancers. *Nat. Med.* **21**, 938–945 (2015).


## Acknowledgements

We thank M. Wilk and J. Barrett for assistance with experiments. This research was supported by National Institutes of Health (NIH) grant R01 AI11304603 (M.B.B.), European Research Council (ERC) Starting Grant 679173, a Cancer Research Institute CLIP grant and 16/FRL/3865 (L.L.).

## Author contributions

X.M., L.D., and L.L. conceived and designed the experiments, and wrote the manuscript. X.M., L.D., A.H., R.M.L., D.D., K.W., R.D., M.R., and L.L. performed the experiments. C.F. performed the RNA-seq analysis. A.T., A.V., W.P., D.O'S., and B.S.N. obtained patient samples and coordinated the clinical investigations. S.B., C.O.F., K.H.G.M., M.B.B., and D.F. provided advice, reagents and critical insight.

## Competing interests

The authors declare no competing interests.

## Additional information

**Supplementary information** is available for this paper at https://doi.org/10.1038/s41590-018-0251-7.

**Reprints and permissions information** is available at www.nature.com/reprints.

**Correspondence and requests for materials** should be addressed to L.L.

**Publisher's note:** Springer Nature remains neutral with regard to jurisdictional claims in published maps and institutional affiliations.

## Methods

**Mice.** Male C57BL/6 mice were purchased from Jackson Laboratory or Harlan Laboratories. For obesity studies, mice were fed a HFD (60% calories from fat, Research Diets) for 8–13 weeks. Mice were bred in our specific-pathogen-free facilities at Harvard Medical School or Trinity College Dublin. All animal work was approved by and in compliance with the Institutional Animal Care and Use Committee guidelines of The Dana Farber Cancer Institute and Harvard Medical School or the Trinity College Dublin university ethics committee and the Health Products Regulatory Authority Ireland.

**B16 tumor model.** Female C57BL/6 mice were purchased from Harlan Laboratories. Mice were co-housed and randomized after tumor induction. The B16F10 mouse melanoma cell line was purchased from the American Type Culture Collection (ATCC). B16 cells ($2\times10^5$ cells per mouse) were injected subcutaneously (s.c.) into the right flank. For HFD studies, mice were fed a HFD (45% calories from fat, Research Diets) for 12 weeks and tumor cells were injected after 10 weeks. For the adoptive transfer studies, mice were injected s.c. with NK cells ($1.2–2\times10^6$ cells per mouse) or PBS into the tumor site on days 3, 7, and 11 post tumor induction. Tumor growth was recorded every 2–3 days and animals were killed when tumors measured 15 mm in diameter (D). Tumor size was calculated using the following formula: $(D1)^2\times(D2/2)$, D1 being the smaller value of the tumor diameter. For flow cytometric analysis, tumors and draining lymph nodes were dissected 15–17 days after tumor induction, and tumors were digested with DNase I (20 units (U) per ml; Sigma-Aldrich) and collagenase D (1 mg ml$^{-1}$; Roche) in RPMI-1460 for 1 h and red blood cells lysed using ammonium chloride lysis buffer. Single-cell suspensions, prepared using a 100 µm nylon mesh, were stimulated with phorbol 12-myristate 13-acetate (PMA; 10 ng ml$^{-1}$; Sigma-Aldrich), ionomycin (500 ng ml$^{-1}$; Sigma-Aldrich) and brefeldin A (BFA; 5 µg ml$^{-1}$; Sigma-Aldrich) for 4 h at 37 °C. Cells were stained with LIVE/DEAD Fixable Aqua Dead Cell Stain (Life Technologies) and fluorochrome-conjugated antibodies for CD45, CD19, CD3, NKp46, and NK1.1, then fixed, permeabilized and incubated with antibodies for IFN-γ and granzyme B. Data were acquired using a LSRFortessaTM (BD) flow cytometer and analyzed with FlowJo v10 software.

**Preparation of NK cells for in vivo transfer.** For expansion of NK cells, single-cell suspensions of murine spleens were prepared and lysed with ammonium chloride lysis buffer. NK cells were cultured in IL-15 (10 ng ml$^{-1}$; Peprotech) and isolated as described previously[12]. On day 6, NK cells were treated with or without lipids (100 µM palmitate + 100 µM oleate; Sigma Aldrich) for 24 h and subsequently activated with IL-12 (25 ng ml$^{-1}$; R&D), IL-15 (50 ng ml$^{-1}$) and IL-18 (5 ng ml$^{-1}$; R&D) for another 18 h without removing the lipids. NK cells were washed in PBS prior to in vivo transfer.

**Microarray.** NK cells were sorted on a FACSAria (BD) by the Flow Cytometry Core of The Dana-Farber Cancer Institute. Cells were double sorted to >95% purity and collected into TRIzol (Invitrogen). Sample processing and data analysis were performed as described previously[45]. Expression plots were produced with GenePattern.

**Human subjects.** Ten milliliters of peripheral blood were obtained from healthy donors and patients with obesity attending the weight loss clinic at Brigham and Women's Hospital, Boston medical Center, or St. Vincent's University Hospital Dublin (mean age 47, range 24–60 years; mean BMI 48). All blood samples were obtained with written informed consent. The ethics committee at Boston Medical Center, Brigham and Women's Hospital, and St. Vincent's University Hospital Dublin, granted approval for this study.

**Cell culture.** Human peripheral blood mononuclear cells were isolated from healthy volunteer donors by ficoll density gradient separation using ficoll-paque (GE Healthcare). Primary NK cells were purified by positive selection using the NK cell purification kit (Miltenyi Biotec). NK cells were then cultured with RPMI 1640 (Life Technologies) supplemented with 10% heat-inactivated fetal bovine serum (Life Technologies), 1 ng ml$^{-1}$ IL-15 (Peprotech). The YT-indy immortalized NK cell line and the human NK target cell lines K562 and 721.221 were cultured in RPMI 1640 medium (Life Technologies) supplemented with 10% heat-inactivated fetal bovine serum (Life Technologies), 100 units (U) per ml penicillin and 100 µg ml$^{-1}$ streptomycin (Life Technologies). The cell culture was performed at 37 °C and 5% $CO_2$. For lipid treatment, stock solutions of sodium palmitate (Sigma-Aldrich) and sodium oleate (Sigma-Aldrich) were made at 25 mg ml$^{-1}$ in methanol. Palmitate and oleate were dried in a glass tube with pulsed air, then resuspended in NK cell culture medium. The lipid solutions were finally gently sonicated for 2 to 5 min in a water bath sonicator. Freshly isolated NK cells were incubated for 36 to 48 h in complete medium supplemented with sodium palmitate (Sigma-Aldrich) or a mixture of sodium palmitate and sodium oleate (Sigma-Aldrich). For cytokine stimulation assays, NK cells were cultured with IL-2 (50 µg ml$^{-1}$) and IL-12 (20 ng ml$^{-1}$) (Peprotech) for 18 h at 37 °C in NK cell culture medium. For mouse PPAR experiments, splenocytes were cultured with low-dose IL-15 (10 ng ml$^{-1}$) in the presence or absence of the agonists for 6 days. For human PPAR studies, purified human NK cells were cultured in low-dose IL-15 (1 ng ml$^{-1}$) in the presence of agonists or antagonists for 5 days. Drugs used to culture NK cells with in this study are: rapamycin (20 or 100 nM; Tocris), Torin 1 (250 µM; Selleck Chemicals), etomoxir (200 µM; Tocris), 2-DG (30 µM; Sigma-Aldrich) SL0101-1 (10 nM; Cayman), PPARα agonist WY14643 (10 µM), PPARδ agonist GW501516 (10 µM), PPARα antagonist GW6471 (10 µM), and PPARδ antagonist GSK3787 (10 µM).

**Antibodies.** Antibodies with the following specificities were obtained from BioLegend: anti-CD2 (RPA-2.10), anti-CD56 (HCD56), anti-IFN-γ (4S.B3), anti-CD107a (H4A3), anti-CD3 (OKT3), anti-PRF-1 (dg9) and anti-granzyme B (GB11). Mouse antibodies: anti-CD45 BV605 (30-F11), anti-CD3 BV650 (17A2), anti-NKp46 BV711 (29A1.4), anti-NK1.1 BV421 (PK136), anti-IFN-γ PerCP/Cy5.5 (XMG1.2). Anti-Perforin (Pf-80/164) was purchased from Mabtech, the anti-Pericentrin from Abcam, the anti-p-S6 (Ser235/236) from cell signaling and the Anti-granzyme B PE-Cy7 (NGZB) from eBioscience. Secondary antibodies donkey anti-mouse and rabbit coupled to fluorescent Alexa probed were purchased from Jackson Immunoresearch.

**Cytotoxicity assay.** For NK cells from blood of obese and lean donors, isolated NK cells were cultured with K562 cells at a ratio of 10:1 for 4 h at 37 °C. NK cell cytotoxicity was determined using the CytoTox-Fluor cytotoxicity assay (Promega), following the manufacturer's instructions. For NK cell cytotoxicity assay by flow cytometry, target cells were labeled with 1 µM CellTraceViolet (Life technologies) or 2 µM CellVue Maroon (Ebioscience) and then mixed with NK cells at various NK:target ratios in NK cell culture medium in a 96-well plate (Corning). Anti-LAMP-1 conjugated with alexa 488 or alexa 647 (BioLegend) and monensin (BioLegend) were added to measure NK degranulation. The cells were then centrifuged to synchronize NK:target conjugate formation and incubated at 37 °C for 1 to 2 h. Cells were then washed with cold PBS. The percentage of dead target cells was measured with propidium iodide (Pi) staining (Sigma Aldrich) by flow cytometry.

**Oxygen consumption rate and extracellular acidification rate measurement.** XF-24 or XFe-96 Extracellular Flux Analyzers (Seahorse Bioscience) were used for measurement of OCR and ECAR. Purified NK cells were plated at $5\times10^5$ cells per well for the 24-well Seahorse or $2\times10^5$ cells per well for the 96-well Seahorse analyzer in Seahorse plates coated with CellTak (BD pharmingen). The OCR and ECAR were measured in XF RPMI Seahorse medium supplemented with 10 mM glucose and 2 mM L-glutamine in response to oligomycin (2 µM), FCCP (1 µM), rotenone (100 nM) plus antimycin (4 µM), 2-DG (30 mM) or etomoxir (200 µM) (Sigma-Aldrich). OXPHOS, glycolysis and glycolytic capacity were calculated as follows:

$$\text{OXPHOS} = [\text{OCR}]_{\text{basal}} - [\text{OCR}]_{\text{rotenone/antimycin A}}$$

$$\text{Maximum respiratory rate} = [\text{OCR}]_{\text{FCCP}}$$

$$\text{Glycolysis} = [\text{ECAR}]_{\text{basal}} - [\text{ECAR}]_{\text{2-DG}}$$

$$\text{Glycolysis capacity} = [\text{ECAR}]_{\text{oligomycin}}$$

$$\text{Spare glycolytic reserve} = [\text{ECAR}]_{\text{oligomycin}} - [\text{ECAR}]_{\text{basal}}$$

**Immunoblot analysis.** For immunoblot analysis, cells were collected, washed twice with ice-cold PBS and lysed at $1\times10^7$ cells per ml in lysis buffer containing 50 mM Tris-HCl pH 6.7, 2% SDS, 10% glycerol, 0.05% bromphenol blue, and 1 µM dithiothreitol. Samples were denatured at 95 °C for 10 min, separated by sodium dodecyl sulfate–polyacrylamide gel electrophoresis and transferred to a polyvinylidene difluoride membrane.

**Flow cytometry and cell sorting.** Single-cell suspensions, of blood or from cell culture, were obtained and incubated with Fc receptor-blocking antibody before being stained on ice. Dead cells were excluded by live/dead staining using 7-AAD, or Zombie Aqua (BioLegend) for fixed and permeabilized cells. For sorting and analysis of NK cells, a dump gate with F4/80 was used to eliminate nonspecific staining. Antibodies conjugated to fluorescein isothiocyanate, phycoerythrin, phycoerythrin-indotricarbocyanine, peridinine chlorophyll protein complex 5.5, allphycocyanin, or allophycocyanin-indotricarbocyanine were as follows: CD45, CD3, NK1.1, NKp46, F4/80, and 7AAD. Intracellular staining was performed using a fixation and permeabilization buffer (eBioscience). For IFN-γ production measurement, cells were treated with brefeldin A (eBioscience). Assessment of glucose uptake was performed by incubation of NK cells with 50 µM 2-NBDG (2-(N-(7-nitrobenz-2-oxa-1,3-diazol-4-yl)amino)-2-deoxyglucose; Life Technologies) in RPMI 1640 (Life Technologies) for 30 to 60 min at 37 °C. Assessment of lipids was performed by incubation of cells with LipidTox

neutral lipid stain (Life Technologies) or Bodipy 495/515 (Life Technologies) as recommended by the manufacturer. Stained cells were analyzed on a FACSCanto I or FACSCanto II cytometer (BD Biosciences). Cell doublets were excluded by comparison of side-scatter width to forward-scatter area. Flow cytometry data were analyzed with FlowJo v10 software (Tree Star).

**Immunostaining and microscopy.** For single-cell imaging, cells were adhered to a 0.1% poly-L-lysine (Sigma-Aldrich) coated glass coverslips by cytospin. For conjugate imaging, NK cells and target cells K562 or 721.221 were co-incubated at a NK:target ratio 2:1 for 20 min. Conjugates were then gently adhered to coated coverslips by centrifugation. Cells were fixed for 15 min in PBS with 3.7% paraformaldehyde (PFA; Electron Microscopy Sciences), washed, incubated for 10 min with 50 mM $NH_4Cl$, permeabilized for 5 min with PBS and 0.2% Triton X100, and then blocked for 30 min with PBS, 10% FBS, and 0.05% Triton X100. Cells were then incubated with the indicated primary antibodies in blocking buffer for 1 h or 18 h then washed and incubated with fluorescent secondary antibodies (Jackson Immunoresearch). Cells were mounted in Fluoro Gel with DABCO (Electron Microscopy Sciences). Cells were analyzed on a Nikon TE2000-U inverted microscope equipped with the laser-scanning C1 confocal system using a Plan Apochromat 60×/1.40 NA oil objective. Image analysis and colocalization quantifications were carried out using National Institutes of Health ImageJ software. The localization of the pericentrin staining at the synapse was used to determine the polarization of NK cells. For each replicate of each experiment, a minimum of 100 NK cells was counted. All images were processed with Adobe Photoshop Software and Adobe Illustrator.

**Statistics.** Results are expressed as the mean ± s.e.m. or ± s.d. The statistical tests used were the unpaired Student's *t*-test using Welch's correction for unequal variances, one-way analysis of variance followed by Tukey's post-hoc test, two-way analysis of variance followed by a Bonferroni test and chi-squared test. $P \leq 0.05$ was considered to denote significance. No data points or mice were excluded.

**Reporting Summary.** Further information on research design is available in the Nature Research Reporting Summary linked to this article.

## Data availability

The data that support the findings of this study are available from the corresponding author upon reasonable request.

## References

45. Cohen, N. R. et al. Shared and distinct transcriptional programs underlie the hybrid nature of iNKT cells. *Nat. Immunol.* **14**, 90–99 (2013).

nature research

Corresponding author(s): Lydia Lynch

# Reporting Summary

Nature Research wishes to improve the reproducibility of the work that we publish. This form provides structure for consistency and transparency in reporting. For further information on Nature Research policies, see Authors & Referees and the Editorial Policy Checklist.

## Statistical parameters

When statistical analyses are reported, confirm that the following items are present in the relevant location (e.g. figure legend, table legend, main text, or Methods section).

| n/a | Confirmed | |
|---|---|---|
| ☐ | ☒ | The exact sample size (*n*) for each experimental group/condition, given as a discrete number and unit of measurement |
| ☐ | ☒ | An indication of whether measurements were taken from distinct samples or whether the same sample was measured repeatedly |
| ☐ | ☒ | The statistical test(s) used AND whether they are one- or two-sided<br>*Only common tests should be described solely by name; describe more complex techniques in the Methods section.* |
| ☐ | ☒ | A description of all covariates tested |
| ☐ | ☒ | A description of any assumptions or corrections, such as tests of normality and adjustment for multiple comparisons |
| ☐ | ☒ | A full description of the statistics including central tendency (e.g. means) or other basic estimates (e.g. regression coefficient) AND variation (e.g. standard deviation) or associated estimates of uncertainty (e.g. confidence intervals) |
| ☐ | ☒ | For null hypothesis testing, the test statistic (e.g. *F*, *t*, *r*) with confidence intervals, effect sizes, degrees of freedom and *P* value noted<br>*Give P values as exact values whenever suitable.* |
| ☒ | ☐ | For Bayesian analysis, information on the choice of priors and Markov chain Monte Carlo settings |
| ☒ | ☐ | For hierarchical and complex designs, identification of the appropriate level for tests and full reporting of outcomes |
| ☒ | ☐ | Estimates of effect sizes (e.g. Cohen's *d*, Pearson's *r*), indicating how they were calculated |
| ☐ | ☒ | Clearly defined error bars<br>*State explicitly what error bars represent (e.g. SD, SE, CI)* |

*Our web collection on statistics for biologists may be useful.*

## Software and code

Policy information about availability of computer code

| | |
|---|---|
| Data collection | FACS Diva has been used to collect flow cytometry data.<br>Wave Desktop version 2.6 has been used to collect Seahorse data. |
| Data analysis | GraphPad Prism 6 has been used to analyze the data.<br>Expression plots were produced with GenePattern.<br>Kegg pathway analysis were analyzed with Kegg software.<br>FlowJo v10 has been used to analyze flow cytometry data.<br>Wave Desktop version 2.6 has been used to analyze Seahorse experiments.<br>ImageJ has been used for confocal images.<br>Powerpoint has been used to edit western blot images.<br>Adobe Photoshop has been used to edit confocal images. |

For manuscripts utilizing custom algorithms or software that are central to the research but not yet described in published literature, software must be made available to editors/reviewers upon request. We strongly encourage code deposition in a community repository (e.g. GitHub). See the Nature Research guidelines for submitting code & software for further information.

## Data

Policy information about availability of data

All manuscripts must include a data availability statement. This statement should provide the following information, where applicable:

- Accession codes, unique identifiers, or web links for publicly available datasets
- A list of figures that have associated raw data
- A description of any restrictions on data availability

*Provide your data availability statement here.*

# Field-specific reporting

Please select the best fit for your research. If you are not sure, read the appropriate sections before making your selection.

☒ Life sciences ☐ Behavioural & social sciences ☐ Ecological, evolutionary & environmental sciences

For a reference copy of the document with all sections, see nature.com/authors/policies/ReportingSummary-flat.pdf

# Life sciences study design

All studies must disclose on these points even when the disclosure is negative.

| | |
|---|---|
| Sample size | Human Samples: When possible a minimum of 10 samples lean and obese were used for each experiment. Number of sample depends preliminary data which were used to calculate power calculations on the minimum sample size. As some samples were used for multiple measurements, for example all samples were used for NK cell levels, so there is increased sample size here as it combined all collections.<br>Mouse studies: Power calculations were used to determine the minimum sample size. For HFD experiments, at least 5 mice per group per experiment were used. For the B16 tumor model, 15 mice (Figure 8B-D) or 5 (Figure 8E-J) mice per group were used.<br>In vitro experiments including lipid and drug treatment were performed each time with at least one obese and one lean matched donor to compare. Experiments were repeated 2-5 times with different donors to verify the phenotype. |
| Data exclusions | Data were excluded when human cells were poor quality, for example decreased viability (>20%) due to the freezing or thawing procedure. Exclusion criteria were not pre-established. No murine data were excluded from the analysis. |
| Replication | All experimental findings were reliably reproduced. In many instances, the experiments have been pooled (as indicated).<br><br>Figure 1: All experiments with different samples were reproducible.<br>Figure 2: Various donors gave reproducible results.<br>Figure 3a-c: 2 to 3 experiments, reproducible.<br>Figure 3d: 10 replicates, 8 were reproducible, 2 didn't show changes phenotype. Thought to be due to extended length of experiment and other possibly due to donor.<br>Figure 3e: 4 replicates, all reproducible.<br>Figure 4a: 3 replicates, all reproducible.<br>Figure 4b-c: 1 to 2 replicates, all reproducible.<br>Figure 4d-e: 2 replicates, all reproducible.<br>Figure 4f: All samples with different donors were reproducible.<br>Figure 5a: 2 replicates, all reproducible.<br>Figure 5b: All samples with different donor were reproducible.<br>Figure 5c-e: 5 replicates, all reproducible.<br>Figure 5e: 3 replicates, all reproducible.<br>Figure 5g-i: All samples with different donors were reproducible.<br>Figure 5j-k: 1 experiment, n=3 (HFD) n=5 (SFD) mice<br>Figure 5l-q: 3 experiments (2 reproducible, 1 failed), 3-4 technical replicates per experiment<br>Figure 6a: 1 experiment, reproducible.<br>Figure 6b-d: 3 replicates, all reproducible.<br>Figure 6e: 1 exemplary experiment of 4, all reproducible.<br>Figure 6f: 4 experiments, all reproducible.<br>Figure 6g: 5 experiments, all reproducible<br>Figure 6h-n: 5 experiments, all reproducible<br>Figure 6o: 4 experiments, all reproducible<br>Figure 7a-b: 4 replicates, all reproducible<br>Figure 7c: All samples with different donors were reproducible<br>Figure 7d: 2 replicates, all reproducible<br>Figure 7e: 1 experiment, reproducible.<br>Figure 7f-g: 3 replicates, all reproducible.<br>Figure 7h: 4 replicates, 3 reproducible, 1 failed.<br>Figure 7i-j: 2 replicates, all reproducible<br>Figure 8a: 4 experiments, reproducible<br>Figure 8b-d: 2 experiments (pooled), reproducible<br>Figure 8e-j: 1 experiment, 5 mice per group |

| | |
|---|---|
| Randomization | Peripheral blood was obtained from healthy donors and obese patients. Healthy lean donors have a BMI ranging from 19-25 while Obese patients have a BMI over 33. For mice, littermate controls were ear punched in order to generate experimental groups. In the B16 tumor model, mice were randomized into groups after tumor cell injection. |
| Blinding | For human samples, when possible, the order of acquiring the sample during imaging and flow cytometry was hidden for the investigator during the acquisition of all samples and the gating of results. The the samples were identified into groups at the stage of entering the data into the statistical package.<br>For mouse experiments, investigators were not blinded during data collection and analysis. |

# Reporting for specific materials, systems and methods

## Materials & experimental systems

| n/a | Involved in the study |
|---|---|
| ☒ | ☐ Unique biological materials |
| ☐ | ☒ Antibodies |
| ☐ | ☒ Eukaryotic cell lines |
| ☒ | ☐ Palaeontology |
| ☐ | ☒ Animals and other organisms |
| ☐ | ☒ Human research participants |

## Methods

| n/a | Involved in the study |
|---|---|
| ☒ | ☐ ChIP-seq |
| ☐ | ☒ Flow cytometry |
| ☒ | ☐ MRI-based neuroimaging |

## Antibodies

Antibodies used

Human:
Anti-CD56-APC (HCD56) / BioLegend / 318310 / #B225195
Anti-IFNγ-Alexa488 (4S.B3) / BioLegend / 502515 / #B197426
Anti-IFNγ-FITC (4S.B3) / BioLegend / 502506 / #B179400
Anti-CD107a-APC (H4A3) / BioLegend / 328620 / #B168399
Anti-CD107a (H4A3) / BioLegend / 328602 / #B156594
Anti-CD3-PerCP Cy5.5 (OKT3) / BioLegend / 317336
Anti-PRF-1-PE (dg9) / BioLegend / 308106 / B160766
Anti-GZMB-FITC (GB11) / BD Bioscience / 560211 / #6168965
Anti-Perforin (Pf-80/164) / Mabtech / 3465-3-250
Anti-Pericentrin (N/A)/ Abcam / ab4448
Anti-p-S6(Ser235/236)-PE (D57.2.2E) / Cell Signaling / 5316 / #7 and #8

Mouse:
Anti-CD19 PE-CF594 (1D3) / BD Biosciences / 562291
Anti-CD45-BV605 (30-F11) / BioLegend / 103139
Anti-CD3-BV650 (17A2) / BioLegend / 100229
Anti-NKp46-BV711 (29A1.4) / BioLegend / 137621
Anti-NK1.1-BV421 (PK136) / BioLegend / 108731
Anti-IFN-gamma-PerCP/Cy5.5 (XMG1.2) / BioLegend / 505821
anti-GZMB-PE-Cy7 (NGZB) / eBioscience / 25-8898-80

Validation

Human antibodies: Validated by manufacturer using human PBMCs
Mouse antibodies: Validated by manufacturer using C57BL/6 or BALB/c splenocytes

## Eukaryotic cell lines

Policy information about cell lines

| | |
|---|---|
| Cell line source(s) | Cells lines K562, YT-INDY and 721.221 were obtained from Dr. Michael Brenner's Lab. Cell line B16.F10 was purchased from the ATCC. |
| Authentication | None of the cell lines have been authenticated. |
| Mycoplasma contamination | Cell lines were not tested for mycoplasma infection. However, Imaging studies with DNA staining (Hoechst) didn't show additional small nucleus that could reveal the presence of mycoplasma. |
| Commonly misidentified lines (See ICLAC register) | No commonly misidentified cell lines were used. |

## Animals and other organisms

Policy information about studies involving animals; ARRIVE guidelines recommended for reporting animal research

| | |
|---|---|
| Laboratory animals | C57Bl/6J (WT) were purchased from Jackson Laboratory and maintained in specific-pathogen-free animal facilities at Brigham and Women's Center for Comparative Medicine. In obesity experiments, male mice were used. Mice were 5-6 weeks old at the start of the experiments. In tumor experiments, C56Bl/6J (WT) female mice purchased from Envigo were used. Mice were 6-8 weeks old at the start of the experiments. All animal work was approved by and was in compliance with the Institutional Animal Care and Use Committee guidelines of Brigham and Women's Hospital and Harvard Medical School, and in Trinity Biomedical Sciences Institute. |
| Wild animals | N/A |
| Field-collected samples | N/A |

## Human research participants

Policy information about studies involving human research participants

| | |
|---|---|
| Population characteristics | Peripheral blood were obtained from healthy donors and obese patients attending the weight loss clinic at Brigham and Women's Hospital, Boston medical Center or St. Vincent's University Hospital Dublin, Ireland (mean age 47, range 24–60 years; mean BMI 48). The ethics committee at Boston Medical Center, Brigham and Women's Hospital, Boston and St. Vincent's University Hospital, Dublin granted approval for this study. |
| Recruitment | We collected patients attending the weight management clinic, and a study coordinator collected blood for all patients that agreed to participate in the study. There was no selection bias, other than they had to have a BMI>30. |

## Flow Cytometry

### Plots

Confirm that:

☒ The axis labels state the marker and fluorochrome used (e.g. CD4-FITC).

☒ The axis scales are clearly visible. Include numbers along axes only for bottom left plot of group (a 'group' is an analysis of identical markers).

☒ All plots are contour plots with outliers or pseudocolor plots.

☒ A numerical value for number of cells or percentage (with statistics) is provided.

### Methodology

| | |
|---|---|
| Sample preparation | Human peripheral blood mononuclear cells were isolated from blood (10ml sample or leukopack collars) by Ficoll density gradient separation using ficoll-paques (GE Healthcare). Primary NK cells were purified by positive selection using the NK cell purification kit (Miltenyi Biotec).<br>For surface staining, cells were washed twice with PBS and filtered through a 70um filter. Cells were then stained with NIR-LIVE/DEAD (Life Technologies) for 20 minutes then washed with PBS, 2% FBS, twice. Cells were then stained with antibodies diluted in PBS, FBS 2% for 0.5 to 1H at 4C. Cells were then washed twice before data collection. For intracellular staining, following surface staining, cells were fixed (20 minutes) and permeabilized (20 minutes) (Ebioscience). Fixed cells were then incubated with antibodies for 0.5 to 1H at 4C. Cells were then washed twice before data collection.<br>For cytokine production assays, cells were stimulated with indicated stimulus and then treated with brefeldin A for 4 to 6 hours before sample processing.<br>For cytotoxic assays, target cells were pre-stained with cell trace violet (Life technologies) or Cell Vue Maroon (Ebioscience). Target and NK cells were then co-incubated together with or without Monensin (Ebioscience) and anti-CD107a antibody for 2 to 4 hours. Two to 5 minutes before data collection, samples were stained with Propidium Iodide.<br>For mice:<br>Spleens and lymph nodes were strained through a 70µm cell strainer and spun. Pellets from all tissues were subjected to red blood cell lysis and subsequently resuspended in flow cytometry buffer (2% FBS and 0.02% NaN3 in phenol-free DMEM) for further staining. Tumors and draining lymph nodes were typically dissected 15-17 days after tumor induction and tumors digested with DNAse I (20 U/ml; Sigma-Aldrich) and collagenase D (1 mg/ml; Roche) in RPMI-1460 for 1H and red blood cells lysed using ammonium chloride lysis buffer. Single cell suspensions, prepared using a 100 µm nylon mesh, were stimulated with phorbol 12-myristate 13-acetate (PMA; 10 ng/ml; Sigma-Aldrich), ionomycin (500 ng/ml; Sigma-Aldrich) and brefeldin A (BFA; 5 µg/ml; Sigma-Aldrich) for 4H at 37ºC. Cells were stained with LIVE/DEAD® Fixable Aqua Dead Cell Stain (Life Technologies) and fluorochrome-conjugated antibodies for CD45, CD19, CD3, NKp46, and NK1.1, then fixed, permeabilized and incubated with antibodies for IFNγ and granzyme B. |
| Instrument | BD Bioscience CANTO I and BD Bioscience CANTO II and BD Bioscience Fortessa |
| Software | BD FACSDIVA and FLOWJO (V10) software were used for data collection and data analysis respectively. |
| Cell population abundance | For cytotoxicity assays, a minimum of 2,000 target cells were recorded per replicate. For others assays, a minimum of 10,000 NK cells were recorded per replicate. For human sample analysis, a minimum of 5,000 NK cells were recorded. For microarray |

analysis, a minimum of 30,000 NK cells were sorted. For tumor studies, B16 cells (2 x 105 cells/mouse) were injected subcutaneously (s.c.) into the right flank. On days 3, 7 and 11 post tumor induction, mice were injected s.c. with NK cells (1.2 – 2 x 106 cells/mouse) or PBS into the tumor site.

Gating strategy

In general: Global cell population is gated on FSC-A/SSC-A. Single cells are gated on FSC-A/FSC-H. When appropriate, live cells - using Aqua or NIR LIVE/DEAD Aqua or NIR - are gated. The dead population is determined using cells pretreated with detergent (Tween20, Triton X100) to induce major cell death as a positive control. NK cells were gated as CD56+/CD3- or NK1.1+NKp46 +CD3- in mice.
The IFNg+ and p-S6+ populations were determine using the corresponding negative population in non-stimulated cells or fluorescence minus one controls.
Cell Trace Violet or Cell vue maroon population were gated using a non stained sample.

☒ Tick this box to confirm that a figure exemplifying the gating strategy is provided in the Supplementary Information.